
A REVIEW OF END-TO-END PRECIPITATION PREDICTION USING REMOTE SENSING DATA: FROM DIVINATION TO MACHINE LEARNING

A PREPRINT

 **Yugong Zeng**

Department of Electrical and Computer Engineering
University of Windsor
401 Sunset Avenue
Ontario, Canada N9B 3P4
zeng26@uwindsor.ca

Jonathan Wu

Department of Electrical and Computer Engineering
University of Windsor
401 Sunset Avenue
Ontario, Canada N9B 3P4
jwu@uwindsor.ca

ABSTRACT

Precipitation prediction has undergone a profound transformation—from early symbolic and empirical methods rooted in divination and observation, to modern technologies based on atmospheric physics and artificial intelligence. This review traces the historical and technological evolution of precipitation forecasting, presenting a survey about end-to-end precipitation prediction technologies that spans ancient practices, the foundations of meteorological science, the rise of numerical weather prediction (NWP), and the emergence of machine learning (ML) and deep learning (DL) models. We first explore traditional and indigenous forecasting methods, then describe the development of physical modeling and statistical frameworks that underpin contemporary operational forecasting. Particular emphasis is placed on recent advances in neural network-based approaches, including automated deep learning, interpretability-driven design, and hybrid physical-data models. By compositing research across multiple eras and paradigms, this review not only depicts the history of end-to-end precipitation prediction but also outlines future directions in next generation forecasting systems.

Keywords Machine learning · Neural networks · Precipitation prediction · Remote sensing

1 Introduction

Precipitation prediction is a cornerstone of modern environmental forecasting, which underpins advanced applications in agriculture, disaster management, hydrology, transportation, and climate policy. To elaborate, accurate rainfall forecasts are essential for mitigating the risks of floods and droughts, managing water resources, guiding agricultural activities, and ensuring public safety during severe weather events. In domains such as aviation, ground transportation, and energy production—particularly renewable sources like wind and solar short- and long-term precipitation forecasts inform real-time decision-making and strategic planning. Moreover, according to the view of scholars in the field of climate change, understanding precipitation patterns directly contributes to assessing ecological risks, food security, and the sustainability of natureLi et al. [2022a]. For these reasons, improving the accuracy and scope of precipitation forecasting has become not only a scientific research direction but also a policy priority.

Since its emergence as a formal scientific discipline in the 19th century, geophysics has steadily evolved from the study of Earth’s physical properties to a multifaceted field encompassing climate dynamics, natural hazard assessment, and hydrological modelingSchröder [2010]. Among its most impactful applications is precipitation prediction, which sits at the intersection of atmospheric physics, environmental monitoring, and computational modeling. As observational capabilities expanded—especially with the advent of remote sensing technologies initially developed for military and cartographic purposes—geophysics began integrating global atmospheric data into weather and climate analysis. The launch of satellite missions such as TIROS-1, POES, and Landsat in the latter half of the 20th century marked a turning point, enabling systematic and high-resolution monitoring of meteorological phenomena. These technological advances

transformed precipitation prediction from an observational science into a quantitatively driven, data-rich enterprise at the core of modern geophysical research and applications.

In parallel, the last century has witnessed significant scientific and technological advancements, particularly in the field of computer science. From Alan Turing's conceptualization of the universal computing machine in the 1940s to the development of programmable digital computers and high-level programming languages, computers became a device capable of automating complex analytical workflows. One of the earliest impactful applications was Numerical Weather Prediction (NWP), where atmospheric equations were discretized and solved using finite-difference methods in early machines. These early NWP systems, while pioneering, required a modular sequence of human-designed steps: data assimilation, feature selection, model formulation, and forecast output—all executed in a highly structured and hand-engineered pipeline.

Following this trajectory, machine learning (ML) emerged as a transformative tool. Starting with Arthur Samuel's work on adaptive systems in the 1950s and Tom Mitchell's formal definition in the 1990s, ML gradually moved into the forecasting domain as data and computational power expanded. With the arrival of large satellite archives and dense ground-based measurements, ML increasingly complemented traditional modeling approaches. More recently, the field has moved toward end-to-end learning paradigms, where models learn to map raw observational data (e.g., satellite images, radar sequences, or time-series measurements) directly to high-level predictions such as rainfall, air quality, or climate anomalies—bypassing manual feature engineering. These models, often built with convolutional, recurrent, or transformer-based neural networks, are trained wholly throughout the pipeline, enabling greater automation, adaptability, and predictive performance in domains where a complex system refuses complete physical characterization Mitchell [1997].

This review traces the conceptual and technological evolution of precipitation prediction, from ancient divination practices and symbolic observation to modern end-to-end deep learning models. By surveying key historical milestones, methodological shifts and emerging research frontiers, we aim to provide a comprehensive view of how precipitation forecasting has evolved across disciplines and modeling paradigms. Special attention is given to the growing role of deep learning models, which represent the latest stage in this centuries-long quest to understand and anticipate one of Earth's most vital atmospheric processes.

2 Basics of precipitation prediction

Precipitation prediction refers to estimating the occurrence, type, intensity, and spatial distribution of drizzle, rainfall, snowfall or other products of atmospheric water vapor over a given forecast horizon. Founded in the disciplines of meteorology, atmospheric physics and hydrology, it combines physical modeling of atmospheric dynamics with observational data analysis to anticipate the evolution of weather systems. The prediction process is inherently multiscale, involving interactions across microphysical processes (e.g., condensation, coalescence), mesoscale dynamics (e.g., convection, orographic lifting) and large-scale climatic drivers such as the El Niño–Southern Oscillation (ENSO) Glantz [2001], Trenberth and Stepaniak [2004].

Historically, early attempts at precipitation forecasting were empirical, relying on heuristic rules derived from observed atmospheric patterns Harper [2024]. With the formalization of the governing equations of fluid motion and thermodynamics, modern meteorology embraced numerical weather prediction (NWP), where the Navier-Stokes equations and related conservation laws are discretized and solved using high-performance computing systems Shukla and Kinter [2006]. These models simulate the time evolution of temperature, humidity, wind and pressure fields to derive precipitation estimates, often supplemented by statistical post-processing to improve accuracy Murphy [1988].

Precipitation prediction is challenged by the chaotic nature of the atmosphere, the nonlinear relationships between variables, as well as the limited resolution of observations and models Kalnay [2002a]. Errors can arise from uncertainties in initial conditions, boundary constraints and model physics, particularly in convective-scale forecasting Zhang et al. [2003]. As a result, forecasting precision tends to decline with an increase in lead time and a decrease in spatial scale. To solve these challenges, recent advances have emphasized the use of data assimilation Houtekamer and Zhang [2016], ensemble modeling Palmer [2000], and machine learning techniques Pinheiro and Ouarda [2025] that enhance model calibration and uncertainty quantification. These developments have gradually reshaped precipitation forecasting from a purely physics-based enterprise into a hybridized discipline that balances theory, data, and computation.

3 Brief introduction of remote sensing

Remote sensing is commonly defined as the measurement and analysis of Earth's surface and atmosphere from a distance, typically through satellite or airborne instruments that record reflected, emitted or scattered electromagnetic radiation

across various spectral bands. Founded at the intersection of physics, geography, and engineering, it draws on sensor technology, radiative transfer theory, and geospatial analysis to observe natural and human systems. The discipline is inherently multiscale, encompassing fine-resolution studies of vegetation or urban form, mesoscale dynamics such as storm systems and global drivers of climate variabilityCampbell and Wynne [2011], Lillesand et al. [2015].

Historically, the practice originated with aerial photography in the early 20th century and expanded through satellite missions such as Landsat, NOAA-AVHRR and MODIS, which provided systematic, global observations of land, oceans, and atmosphereIrons et al. [2012]. These platforms transformed remote sensing from a tool for reconnaissance into a scientific enterprise, supporting applications in agriculture, hydrology, climate research, and disaster management. Advances in spectral resolution, spatial coverage and computational methods shifted the field from visual interpretation toward digital image processing, atmospheric correction and automated classificationRichards [2014].

In recent years, remote sensing has increasingly moved beyond simple observation to become a central tool for environmental monitoring and Earth system science. Advances in multispectral, hyperspectral, and radar technologies now provide unprecedented detail across land, ocean, and atmospheric domains. Combined with large-scale data assimilation and machine learning approaches, these developments are enabling new insights into climate variability, ecosystem dynamics, urbanization, and natural hazard assessmentZhu et al. [2018], Reichle et al. [2002], Ma et al. [2019]. As a result, remote sensing has evolved into a cornerstone discipline that integrates theory, data, and computation, supporting both scientific discovery and practical decision-making across a wide range of applications.

4 End-to-end prediction

End-to-end (E2E) prediction refers to a modeling paradigm in which a single computational system learns to map raw input data directly to a target output, without relying on handcrafted intermediate steps or domain-specific feature engineering. Unlike traditional workflows that rely on sequential, modular stages—such as manual feature engineering, statistical pre-processing, and separate prediction models, end-to-end systems optimize the entire workflow jointly, using data-driven learning to determine which representations and transformations are most effective for the prediction task. This approach has gained substantial traction in fields where high-dimensional, unstructured data (such as images, time-series, or multi-sensor arrays) are abundant, and where the relationships between input and output are nonlinear and complex.

In the atmospheric and environmental sciences, E2E methods have shown promise across a spectrum of forecasting challenges. In weather prediction, models such as 3D neural networksBi et al. [2023a] and MetNetSønderby et al. [2020] learn directly from multi-source observational data to produce high-resolution, short-term forecasts without costly numerical integration. For tropical cyclones, spatio-temporal deep networks have been applied to satellite imagery for predicting storm tracks, landfall locations, and rapid intensification eventsGujral et al. [2023], Gan et al. [2024]. Wildfire forecasting now incorporates vegetation indices, meteorological conditions, and satellite-based fire detections into deep learning architectures that capture both ignition risk and spread dynamics Shadrin et al. [2024], Xiao et al. [2024]. Similarly, flood and hydrological forecasting leverages precipitation, soil moisture, and surface water data from missions like GPM, SMAP, and Sentinel-1 to train models capable of real-time flood risk estimationBelabid et al. [2019], Zhang et al. [2025]. Across these applications, E2E approaches reduce reliance on handcrafted physical parameterizations, offer rapid inference, and demonstrate strong adaptability to diverse data sources—positioning them as a transformative complement to traditional physics-based methods.

5 Literature survey

5.1 Ancient predictive methods

Centuries ago, meteorological prediction was largely imprecise and relied heavily on intuition, local climatology, and empirical rules. Observational data were sparse, especially over oceans and in the upper atmosphere, and theoretical physics played little role in practice. Predictions were produced by plotting surface observations on weather maps and manually identifying patterns.

Inasmuch as there was a lack of support from theoretical physics, ancient weather forecasting was based more on observation, symbolism, and cultural practices than scientific reasoning. Dating back to the 7th century BCE, Babylonian scholars reported rain or drought based on astronomical diariesRochberg [2004]. In ancient Greece, Aristotle's *Meteorologica* (circa 340 BCE) took this empirical meteorology a step further. His approach to meteorology was characterized by deductive reasoning, using observed weather phenomena not to form hypotheses, but to validate pre-existing theoretical frameworksWilson [2013]. Chinese meteorological records from the Han Dynasty (around 200 BCE) included solar and lunar observations, which were correlated with seasonal climate variationsNeedham and

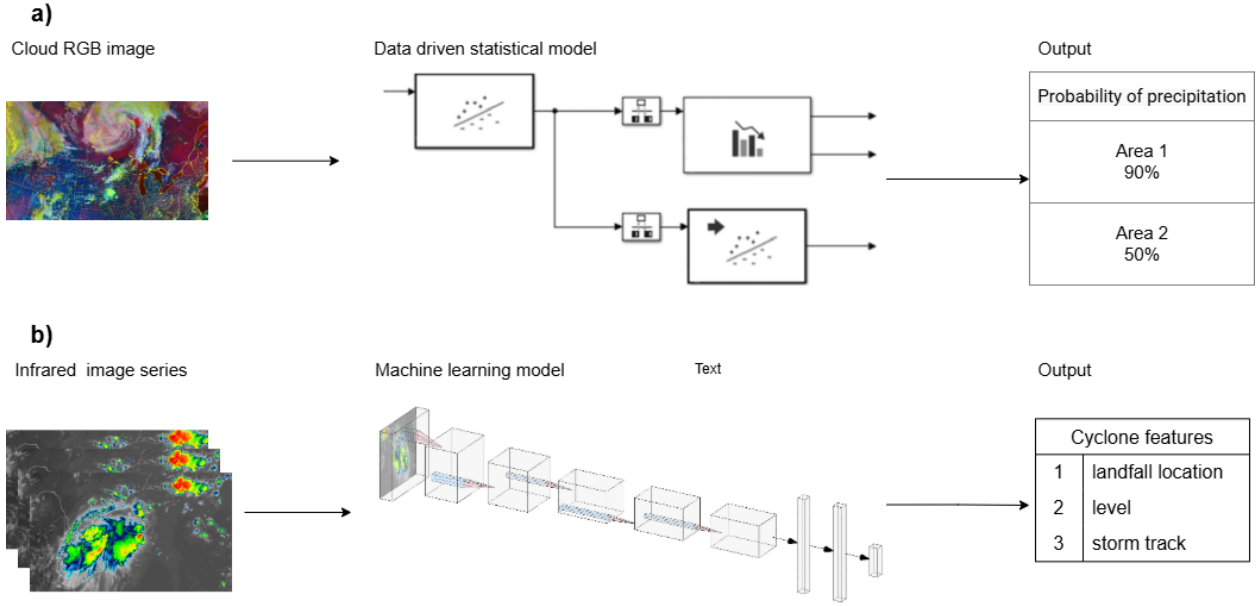


Figure 1: E2E prediction models in atmospheric application. a) Statistical mode. b) Machine learning model.

Ling [1959]. scholars such as Al-Battani and Ibn al-Shatir refined astronomical instruments, including the astrolabe, which indirectly supported climatological assessments Saliba [2007]. In medieval Europe, forecasting relied on folklore and almanacs that linked celestial events, such as eclipses or moon phases, with weather changes. Although these approaches are regarded as unscientific by modern standards, they represent early efforts to formalize atmospheric observation and forecast Campion [2009].

5.2 Foundation of meteorological precipitation prediction

With the development of theoretical physics and astronomy, in the last decade of 19th century, early pioneers such as Cleveland Abbe and Vilhelm Bjerknes articulated the foundational principles of scientific weather prediction, with Bjerknes proposing a systematic framework involving both diagnostic and prognostic steps based on governing equations of the atmosphere Friedman [1989]. This vision was carried forward by Lewis Fry Richardson, who attempted the first numerical weather forecast in 1917 using finite difference approximations. Although his effort resulted in unrealistic outcomes due to data imbalance and the absence of computational tools, it introduced the core concept of modeling atmospheric evolution via numerical integration of physical equations Lynch [2008a].

The practical realization of Richardson's concept began in the mid-20th century, catalyzed by advances in atmospheric theory, observational systems, and digital computing. Led by a meteorologist, Jule Charney, the first successful computer-generated forecasts were executed on the ENIAC (Electronic Numerical Integrator and Computer) in 1950 to solve the barotropic vorticity equation. Due to the limited internal memory capacity of ENIAC, a relatively large space interval of 736 km constituted the forecasted grid rectangle. Another notable record is that the time interval for this 24-hour forecast was also 3 hours Weik [1961]. Two years later, the UK Met Office integrated a baroclinic model with a vertically uniform thermal wind. The enhanced model improved the resolution to 260 km and reduced the time interval to 1 hour. These pioneering efforts demonstrated the feasibility of simulating large-scale atmospheric flow patterns. However, these models treated the atmosphere as a 2-dimensional fluid on a constant pressure surface, limiting their ability to represent vertical structure. By 1955, the Joint Numerical Weather Prediction Unit (JNWP) in the United States introduced a 3-layer barotropic model over the Northern Hemisphere, enhancing vertical resolution. This was followed by the short-lived thermotropic model in 1956, which incorporated two layers and temperature gradients, marking an early step toward representing baroclinic processes. The breakthrough came in 1966, when the United States implemented operational primitive equation models, which included full 3-dimensional dynamics across vertical levels (as shown in Table 1). These primitive equation models, based on the full set of hydrostatic and thermodynamic governing equations, represented a major leap in realism by simulating the vertical and horizontal transport of mass, momentum, heat, and moisture. Based on primitive equations, in 1974, the U.S. National Weather Service deployed a 9-layer global forecast model on IBM, marking the first global-scale NWP with more complete physics—radiation,

Year	Location/Agency	Model Type	Computing Platform	Comment
1950	Aberdeen, USA	Barotropic vorticity equation (single-layer, 3-hour time-step, 736 km space interval)	ENIAC	The first successful numerical prediction Lynch [2008b], Charney et al. [1950]
1952	UK (Met Office)	Barotropic model (single-layer, 1-hour time-step, 260 km space interval)	EDSAC and LEO computers	Solved height tendency equations Golding et al. [2004]
1954	Sweden (International Meteorological Institute)	Barotropic model (single-layer)	BESK	First real-time barotropic forecast Harper et al. [2007]
1955	USA (JNWP)	Barotropic model (3-layer, Northern Hemisphere only)	IBM 701	First introduction of multi-level structure Nebeker [1995]
1956	USA (JNWP)	Thermotropic model (2-layer)	IBM 701	First introduction of temperature effects Nebeker [1995]
1959	Japan (JMA)	Barotropic model (single-layer)	IBM 704	First Northern Hemisphere barotropic model in Asia Persson [2005]
1960	Australia	Barotropic model (single-layer)	DEUCE type computer	First real-time numerical forecast in the Southern Hemisphere Persson [2005]
1966	USA (NMC)	Primitive equation model (6-layer)	CDC 6600	First implemented primitive equations Lynch [2008a]
1974	USA (NWS)	Global forecast model (9-layer)	IBM 360, Cray I	First global-scale NWP model with complete physics

Table 1: Historical milestones in early numerical weather prediction (NWP)

moist processes, and boundary-layer parameterizations—thereby establishing the blueprint for modern operational global models.

5.3 Development of meteorological precipitation prediction

The development of global meteorological prediction models has seen remarkable advancements since the early 1980s, primarily driven by breakthroughs in numerical methods and the rapid growth of computational capacity. A foundational step came in 1980 when the U.S. National Meteorological Center (NMC) introduced the Global Spectral Model (GSM), employing spectral transform techniques to enhance the accuracy of medium-range weather forecasts, including quantitative precipitation forecasts Kalnay [2002b], Krishnamurti et al. [1998]. This marked the first operational implementation of a primitive equation-based global model in the United States. Building on this progress, the European Center for Medium-Range Weather Forecasts (ECMWF) launched its own high-resolution spectral model in 1985, establishing itself as a global leader in medium-range forecasting skill. It quickly became a global benchmark in medium-range precipitation prediction, owing to its superior numerical stability and representation of moist physical processes Palmer [2019]. Around the same period, the UK Met Office began operational runs of its Unified Model in the late 1980s, a flexible system designed to serve both global and regional forecasting needs within a single modeling framework, including precipitation driven by convective and stratiform processes Golding et al. [2004]. Canada followed suit in 1991, introducing its Global Deterministic Prediction System (GDPS), transitioning from hemispheric to full global coverage, which significantly improved precipitation forecast accuracy across diverse climatic regions.

By the 2000s, the scope and complexity of global precipitation forecast systems expanded further. The United States had previously relied on separate models for different forecast ranges—namely, the Medium Range Forecast (MRF) and Aviation (AVN) models—but these were unified into the Global Forecast System (GFS) in 2002. The GFS provided seamless forecasts up to 16 days and incorporated various Earth system components, including land surface, sea ice, and radiation processes. That same year, the German Weather Service (DWD) implemented the Global Model (GME), becoming the first agency to adopt an icosahedral–hexagonal grid, enhancing precipitation prediction in polar regions by removing grid singularities. In pursuit of even greater resolution and computational efficiency, NOAA developed the Flow-following, finite-volume Icosahedral Model (FIM) in the mid-2010s as a potential successor to the GFS. These

global efforts illustrate a coordinated international shift toward unified, high-resolution, and fully coupled Earth system models, enabling more skillful precipitation predictions across spatial and temporal scales, and forming the backbone of modern operational forecasting.

While Numerical Weather Prediction (NWP), initiated in the mid-20th century, relies on solving the physical equations governing atmospheric dynamics, its limitations—especially in short-range or local-scale forecasts—prompted the development of statistical post-processing methods. In 1972, Harry R. Glahn and Dale A. Lowry introduced Model Output Statistics (MOS) with screening regression into weather forecasting, specifically, probability of Precipitation (Pop)Glahn and Lowry [1972]. They denoted a predictand \hat{Y} as a linear combination of independent predictors, named X_0 to X_k :

$$\hat{Y} = a_0 + a_1 X_1 + a_2 X_2 + \dots + a_k X_k$$

Where a_i is called the coefficients. Then, they applied root mean square error (RMSE) on dependent sample of size n to determine the goodness of the equation for estimation.

By leveraging screening regression, which iteratively selecting a parsimonious subset that minimizes estimation error, they derived a statistically optimized equation that translated NWP-derived predictors. This method significantly outperformed climatological and persistence-based forecasts, and also addressed key limitations of raw model outputs by accounting for systematic biases and local climatological characteristics. In 1990, Jan John and Josef Štekł expanded their framework into nonlinear adaptive regression predictors, based on singular value decomposition (SVD)John and Štekł [1990]. In this adaptive framework, SVD serves both as a numerical stabilizer and an implicit screening mechanism, effectively filtering out low-information components (e.g., redundant predictors) while preserving the signal-bearing directions in the data. While adaptive regression for temperature showed promise, Singular Value Decomposition (SVD) was soon applied specifically to precipitation prediction. For example, Liu developed a forecast model by applying a lagged SVD between soil moisture fields and subsequent monthly–seasonal precipitationLiu [2003]. The approach yielded skillful regional precipitation forecasts, underpinning the utility of SVD methods for dynamically informed, data-driven rainfall prediction. The success of these early approaches underscored the value of combining physical model outputs with data-driven statistical corrections—a philosophy that laid the foundation for modern ensemble post-processing and machine learning-based forecasting techniques.

5.4 Modern technologies: introduction of datasets

Building on these statistical foundations, modern society has been witnessing extensive applications of machine learning in precipitation prediction. These approaches marked a paradigm shift from linear regression-based frameworks toward models capable of capturing nonlinear relationships within high-dimensional atmospheric data. A key factor of this transition has been the increasing availability of large-scale, high-quality datasets which provide spatio-temporally consistent records of atmospheric variables for training and benchmarking. Therefore, we concluded a series of the most commonly used datasets prior to introducing machine learning models.

5.4.1 ERA5

ERA5 (ECMWF Reanalysis v5), the fifth-generation global atmospheric reanalysis, produced by the Copernicus Climate Change Service (C3S) at ECMWF, spans from January 1940 to the presentSoci et al. [2024]. It delivers hourly estimates of a wide array of atmospheric, land-surface, and ocean-wave variables on a global 31 km grid (0.25°). Vertically, ERA5 resolves the atmosphere on 137 hybrid model levels up to about 1 hPa, with additional products interpolated to 37 pressure levels. In addition to the high-resolution deterministic product (HRES), ERA5 includes a 10-member ensemble of data assimilations (EDA), available at reduced spatial (63 km) and temporal (3-hourly) resolution, which provides flow-dependent uncertainty estimates. The observing system assimilated in ERA5 has expanded from 17,000 reports per day in 1940 to 25 million per day in 2022, reflecting the incorporation of aircraft, balloon-borne instruments, buoys, ships, and satellite observations. Accordingly, the quality of the reanalysis improves substantially throughout the record. Recent refinements include improved treatment of tropical cyclone observations from the International Best Track Archive for Climate Stewardship (IBTrACS) and bias correction of surface pressure records, leading to a more homogeneous representation of extreme events and soil moisture consistency.

In addition, ensemble mean and spread are directly accessible to quantify uncertainty, and the dataset is updated in near-real time with a latency of about five days. Preliminary products are subsequently replaced by final quality-controlled versions after two to three months, ensuring both timeliness and reliability for climate and forecasting applications. Although uncertainties remain in the early decades, particularly over the Southern Hemisphere where observations were sparse, ERA5 provides a long, high-resolution, and physically consistent record of atmospheric variables which serves as both a benchmark and a key training dataset for modern machine learning models in precipitation prediction.

5.4.2 SEAS5

The ECMWF Seasonal Forecasting System 5 (SEAS5) is the fifth-generation global seasonal prediction system, operational since November 2017, designed to provide subseasonal-to-seasonal (S2S) climate outlooks Johnson et al. [2019]. SEAS5 is based on ECMWF's Integrated Forecasting System (IFS), closely aligned with the model cycle used in medium-range forecasts, but configured for longer integrations. Currently, SEAS5 issues ensemble forecasts with 51 members initialized on the first day of each month. Each forecast extends 7 months ahead, with an additional extended set of 15 members initialized once per quarter that run up to 13 months ahead. This ensemble framework captures forecast uncertainty and allows for robust probabilistic prediction. Horizontally, SEAS5 operates at an approximate 36 km resolution in the grid spacing and 0.25° ocean resolution, with 91 vertical levels up to 0.01 hPa in the atmosphere and 75 vertical levels in the ocean (NEMO model). The system assimilates ocean and atmosphere observations for initialization, and it includes interactive sea ice and land surface components.

Relative to its predecessor (System 4), SEAS5 introduced improved El Niño–Southern Oscillation (ENSO) prediction skill, more realistic sea-ice initialization, better representation of stratospheric processes and upgraded ocean physics. These improvements enhance forecast reliability for precipitation, temperature anomalies, and extreme-event probabilities on seasonal timescales. SEAS5 outputs, including ensemble-based forecasts of precipitation anomalies, are widely used to support seasonal precipitation prediction in hydrology, agriculture, energy and disaster risk management, and are publicly available via the Copernicus Climate Data Store.

5.4.3 GOES Satellite Imagery Dataset

The Geostationary Operational Environmental Satellites (GOES) program, operated by NOAA in partnership with NASA, provides continuous geostationary observations of the Western Hemisphere. Since the launch of the GOES-R series (GOES-16 in 2016, GOES-17 in 2018 and GOES-18 in 2022), the primary instrument, the Advanced Baseline Imager (ABI), has delivered high-resolution multispectral imagery across 16 spectral bands, including visible, near-infrared, and infrared channels.

GOES ABI imagery is produced at spatial resolutions of 0.5 km (visible), 1 km (near-IR), and 2 km (IR bands), with temporal refresh rates of 5–10 minutes for full-disk coverage, 15 minutes for hemispheric scans, and as frequent as 30–60 seconds in mesoscale sectors. Among these, the infrared channels (10–12 μ m) are especially important for precipitation-related applications, as they provide cloud-top brightness temperature information that correlates with convective activity.

While GOES imagery itself represents radiance and brightness temperature fields, it serves as the basis for numerous precipitation estimation algorithms and products. Examples include the Hydro-Estimator (HE), the GOES Rainfall Rate/Quantitative Precipitation Estimate (RRQPE), and multi-sensor merged products such as IMERG, which incorporates GOES IR data to improve temporal sampling.

Accordingly, GOES imagery is widely used in nowcasting, extreme weather monitoring, and as an input feature for machine learning models aimed at precipitation prediction. Its combination of high spatial resolution, rapid refresh rates and long-term continuity (dating back to the first GOES in 1975) makes it a cornerstone observational dataset for precipitation science in the Americas.

5.4.4 PRISM

The Parameter-elevation Regressions on Independent Slopes Model (PRISM) dataset, developed by Oregon State University, provides high-resolution gridded climate data for the conterminous United States Daly et al. [2021]. PRISM datasets cover multiple variables, with precipitation (rain + melted snow) as a primary element. PRISM precipitation products are available at a spatial resolution of 4 km, with multiple temporal aggregations, including daily, monthly, seasonal and annual means, extending back to 1895 for long-term climate monitoring. The methodology uniquely incorporates climatologically aided interpolation, in which short-term records are combined with long-term normals to reduce bias and ensure temporal consistency. Precipitation fields incorporate gauge data from diverse sources (e.g., COOP, SNOTEL, CoCoRaHS, USCRN), with radar (NCEP Stage II/IV and later MRMS) blended into the interpolation framework since 2002 for the central and eastern United States.

PRISM datasets are widely validated and recognized for their superior performance in complex terrain, especially in the western U.S., where orographic gradients are pronounced. As such, PRISM is often considered the “climate dataset of record” for U.S. agencies, supporting applications in hydrology, ecology, agriculture, and climate change assessment.

For precipitation prediction research, PRISM serves a dual role. Firstly, it serves as a benchmark reference dataset for validating machine learning models and downscaling approaches. Its second role is an input training dataset which provides long, consistent and high-resolution precipitation records across diverse physiographic regimes.

5.4.5 IMERG

IMERG (Integrated Multi-satellitE Retrievals for GPM), developed jointly by NASA and JAXA under the GPM mission, provides a globally consistent, high-resolution precipitation dataset Huffman et al. [2020]. IMERG merges observations from a constellation of passive microwave sensors aboard multiple satellites, calibrated with the GPM Core Observatory’s dual-frequency precipitation radar (DPR) and microwave imager (GMI). Infrared observations are also incorporated to enhance temporal sampling. IMERG provides precipitation estimates on a $0.1^\circ \times 0.1^\circ$ latitude-longitude grid (10 km) at 30-minute temporal resolution, with global coverage between 60°N - 60°S (and partially outside of that latitude band). Data are released in three latency modes: Early Run (4-hour delay), Late Run (14-hour delay), and Final Run (3.5-month delay). The dataset also includes uncertainty estimates, probability fields (e.g., probability of liquid precipitation phase), and quality indices.

IMERG data have been extensively validated against rain gauge networks worldwide and demonstrate robust skill across a range of climatic regimes, though challenges remain in capturing extremes and solid precipitation. Its combination of fine spatio-temporal resolution, long record and near-real-time availability makes IMERG a cornerstone dataset for both operational applications (e.g., disaster monitoring, flood forecasting) and research contexts, including training and evaluation of machine learning models for precipitation prediction.

5.4.6 SEVIR

The SEVIR (Storm EVent ImagRy) dataset is a large-scale, curated benchmark for applying deep learning to meteorological imaging tasks such as precipitation nowcasting, synthetic radar generation and storm classification Veillette et al. [2020]. SEVIR aims to integrate multiple sensing modalities into a spatio-temporally aligned dataset designed to accelerate research in weather and climate prediction. SEVIR consists of image sequences over 10000 weather events across the contiguous United States (CONUS), each covering a $384\text{ km} \times 384\text{ km}$ patch and a 4-hour temporal window. The dataset includes five complementary data types: three channels (i.e., C02, C09, C13) from the GOES-16 Advanced Baseline Imager, vertically integrated liquid radar mosaics from NEXRAD (Next-Generation Radar) and lightning flashes from the GOES-16 Geostationary Lightning Mapper (GLM). This multimodal alignment enables studies of cross-sensor relationships between cloud dynamics, radiative properties, precipitation structure and convective activity. The dataset’s design addresses the major challenges of using raw GOES and NEXRAD archives—namely, data volume, alignment complexity, and the scarcity of machine-learning-ready benchmarks. Stored in HDF5 format with detailed metadata and an event catalog, SEVIR facilitates reproducible model training and evaluation. It has since become one of the most widely adopted resources for benchmarking deep neural architectures, especially in precipitation nowcasting and spatio-temporal generative forecasting.

5.5 Modern technologies: models

5.5.1 ANN and DNN based models

The earliest applications of machine learning in remote sensing emerged during the late 1980s and 1990s, primarily through the adoption of artificial neural networks (ANNs) for image classification tasks. These models, inspired by biological neurons, provided a flexible framework for mapping input features, such as multispectral reflectance values, to land cover categories. In 1993, Chen et al. proposed a 4-layer ANN model on rainfall prediction using geostationary meteorological satellite (GMS) image sets of Shikoku, Japan Chen and Takagi [1993]. They introduced T_{cov} and T_{mfd} to complement infrared temperature (IR) and visible image graylevel (VIS) as input features (shown in fig 2).

In detail, T_{cov} represents the division of variation and the average of the 2° length region, while T_{mfd} represents the average of difference between NW-SE and NE-SW within 3 grid distances. The proposed network has 2 hidden layers, possessing the ability to sort the relationships with the input data (e.g., infrared band, visible band, and input features). During the training process, rainfall intensity of ground true radar was used as the teacher signal, with randomly selecting half of the original GMS images as a training set. By reducing the rainfall intensity to 4 levels, the model achieved a converged output with a good degree of intensity differentiation. They got a 90.45% accuracy score in validation data, comparing higher than regression based conventional methods. 4 years later, Hsu et al. developed a system for precipitation estimation from remotely sensed information using artificial neural networks (PERSIANN) lin Hsu et al. [1997], which was designed to adjust to geographical and seasonal variability in rainfall patterns, and produced high-resolution rainfall estimates at both hourly and monthly scales. In their research, a modified counter propagation network (MCPN) with two main components, i.e. self-organizing feature map (SOFM) and modified Grossberg linear layer (MGLL), is adopted to estimate rainfall rate from the single input—satellite infrared (IR) imagery. The SOFM layer performs unsupervised clustering of the input spatial features as $T_b^1, T_b^3, T_b^5, SDT_b^3, SDT_b^5$ and $SURF$ shown in Figure 3, selecting a winning node by computing the Euclidean distance d_j between the input vector $(x_i^o; i = 1, \dots, n_0)$ and each node’s weight vector w_{ji} . The prediction pipeline is as follows:

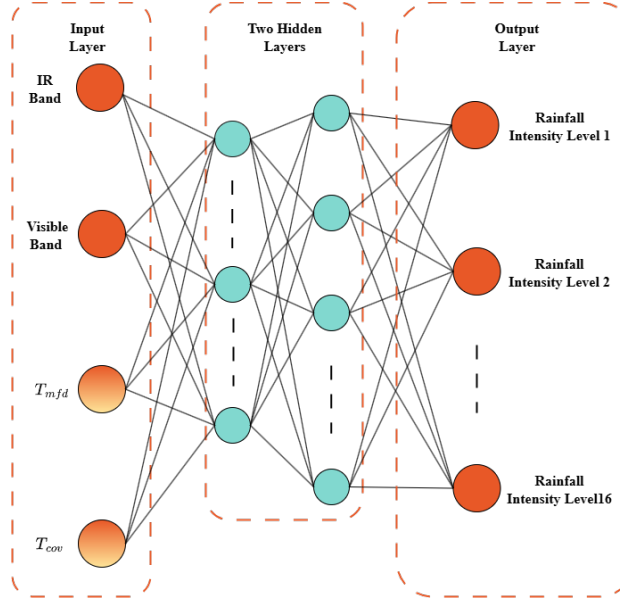


Figure 2: ANN Model by Chen et al. Chen and Takagi [1993].

Algorithm 1 SOFM–MGLL Based Rainfall Prediction

Require: Training set $\{(\mathbf{x}^o, z^o)\}$ with features $\mathbf{x}^o = [T_b^1, T_b^3, T_b^5, SDT_b^3, SDT_b^5, SURF]$; SOFM weights $\{\mathbf{w}_j\}$; MGLL weights $\{v_{kj}\}$; learning rates $\eta \in (0, 1)$, $\beta \in [0, 1]$; neighborhoods Λ_c (SOFM), Ω (MGLL).

Ensure: Predicted rainfall \hat{z} for a new input \mathbf{x}

1: **for** each training sample (\mathbf{x}^o, z^o) **do**

2: **SOFM competition:** Compute

$$d_j \leftarrow \|\mathbf{x}^o - \mathbf{w}_j\|_2, \quad \forall j$$

3: Select winning node: $c \leftarrow \arg \min_j d_j$

4: **SOFM adaptation:** For $j \in \Lambda_c$, update

$$\mathbf{w}_j \leftarrow \mathbf{w}_j + \eta(\mathbf{x}^o - \mathbf{w}_j)$$

5: **Intermediate activation:**

6: **if** $j \in \Omega$ centered at c **then**

$$y_j \leftarrow 1 - d_j$$

8: **else**

$$y_j \leftarrow 0$$

10: **end if**

11: **MGLL forward:** For $k = c$, compute

$$z_k \leftarrow \sum_{j \in \Omega} v_{kj} y_j$$

12: **MGLL learning:** For $k = c, j \in \Omega$, update

$$v_{kj} \leftarrow v_{kj} + \beta(z_k^o - z_k)y_j$$

13: **end for**

14: **Inference:** For new input \mathbf{x} , repeat steps 1–6 (skip updates) to obtain \hat{z}

15: **return** \hat{z}

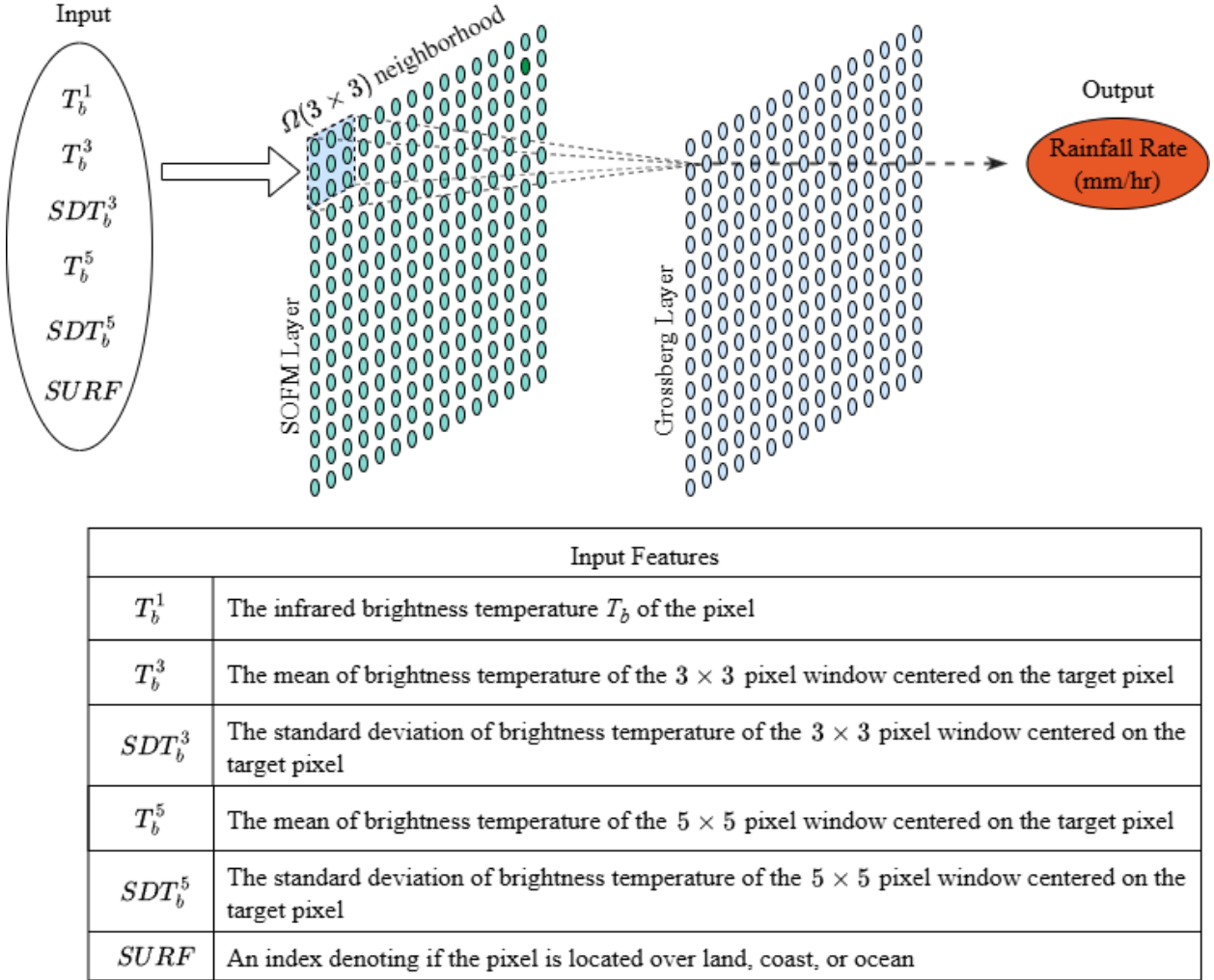


Figure 3: PERSIANN Model by Hsu et al. in Hsu et al. [1997].

In the assessment process, they studied rainfall patterns in Japan and Florida, and leveraged correlation statistic (CORR) and RMSE to validate the model's performance. Also, for further investigation of the MGLL layer, the proposed model was tested in 2 modes, i.e., non-adaptive mode and adaptive mode, distinguished by the parameters v_{kj} updated with each new piece of input data or not. By comparing with a baseline method—the GOES precipitation index (GPI)Meisner and Arkin [1987], the model with adaptive MCPN outperforms the others, e.g., CORR increases from 0.61 (GPI) to 0.88 (adaptive MCPN) as RMSE drops from 101.4 mm (GPI) to 55.36 mm when comparing observed and estimated accumulated rainfall in June 1989 of Japanese islands. Furthermore, they demonstrated the model's capability to learn from sparse data and maintain strong performance when updates occur only every 6–12 hours, simulating limited satellite passes.

In recent years, ANN has still played an important role in rainfall prediction, with some improved variant methods being used. Ahuna et al. presented and validated a backpropagation artificial neural network for short-term rainfall rate prediction with a primary focus on mitigating rain fade over Earth-satellite communication linksAhuna et al. [2017]. The goal of their network is to predict a rainfall rate $x(t + 1)$ estimated by the following expression,

$$x(t + 1) = f(x(t), x(t - 1), x(t - 2))$$

where $x(t)$ is the current rainfall rate, $x(t - 1)$ and $x(t - 2)$ are previous rainfall rates at time $(t - 1)$ and $(t - 2)$ respectively. The backpropagation training algorithm consists of two main phases, named forward pass and backward

pass. In forward pass, the output of a neuron in the hidden layer is determined by the formula,

$$net_{hj} = b_{hj} + \sum_{i=1}^I w_{ji} x_i$$

where net_{hj} is the net output of the j th neuron, x_i is the i th input, w_{ji} and b_{jh} are the weight from i th input and bias to the corresponding neuron respectively. As commonly adopted in machine learning, the training process of backward pass used gradient descent to minimize mean squared error (MSE), while each weight update is determined by the magnitude of the error on actual outputs y_j and the learning rate η , denoted as $\Delta w_i = \eta \frac{\partial E}{\partial y_j}$. Through experimental trials, the authors identified a 3:5:1 architecture (three input neurons, five hidden neurons, and one output neuron) as optimal, achieving a best MSE of 1.1063 at epoch 30. Overall, this model successfully provided an approach for real-time rainfall prediction based on an earth-satellite link.

Deep Neural Networks (DNNs) are a subset of ANNs distinguished by their depth—typically defined as having multiple (often more than three) hidden layers. The additional layers allow DNNs to learn hierarchical feature representations: lower layers capture simple patterns, while deeper layers combine them into increasingly abstract features. For instance, Peng et al. extended the capabilities of artificial neural network-based precipitation models by integrating an automatic hyperparameter optimized framework into a deep neural network architecture Peng et al. [2022a]. This approach systematically searched the parameter space—covering layer configurations, learning rates, and regularization settings—to identify optimal combinations that maximize predictive skill. Compared with manually tuned ANNs, the optimized model demonstrates improved accuracy and robustness, highlighting how automated optimization can mitigate human bias in model design and enhance generalization across varying precipitation regimes. Such a method exemplifies a practical pathway for advancing ANN-based forecasting systems, and provides a scalable means to refine network architectures as datasets, climatic conditions and computational resources evolve. This hierarchical representation enables a DNN-based system to outperform at modeling complex and non-linear relationships in high-dimensional data. In theory, deeper models should exceed shallow ones thanks to greater representational power and hierarchical feature learning ability. However, Rayudu et al. demonstrated a comparison of rainfall prediction ability between ANN and DNN, with a counterintuitive finding that the ANN surpassed the DNN in predictive accuracy for rainfall Rayudu and Roseline [2023]. The study attributes this surprising outcome to several plausible factors: the shallow ANN may have been better optimized for the available data volume, avoided overfitting more effectively than its deeper counterpart, and required less computational overhead, which makes it easier to train and tune. In conclusion, the trade-off is that DNNs require significantly more training data, computational resources, and careful regularization to avoid overfitting. While DNNs often transcend shallow ANNs in tasks with large, complex datasets (such as image recognition or natural language processing), simpler ANNs can be more effective in cases with limited data, lower noise, or when model interpretability and training efficiency are priorities.

5.5.2 KNN based models

k nearest neighbors (KNN), a method that combines the advantages of statistics and early neural networks, originally introduced as a non-parametric, instance-based classifier by Cover and Hart Cover and Hart [1967]. It operates on the principle that similar instances exist in close proximity within the feature space. In its simplest form, KNN assigns a class \hat{y} to a given data point x based on the majority class of its k nearest neighbors, determined by a chosen distance metric. The main calculation process is as follows:

Algorithm 2 K-Nearest Neighbors (KNN)

Require: Dataset $D = \{(x_i, y_i)\}_{i=1}^n$, query point x , number of neighbors k

Ensure: Predicted value \hat{y}

- 1: **for** each $i = 1$ to n **do**
- 2: Compute distance $d_i \leftarrow \|x - x_i\|$
- 3: **end for**
- 4: Identify $\mathcal{N}_k(x) \subset D$: the k samples with the smallest d_i
- 5: **if** task is classification **then**
- 6: $\hat{y} \leftarrow \arg \max_{c \in \mathcal{C}} \sum_{(x_i, y_i) \in \mathcal{N}_k(x)} \mathbb{I}(y_i = c)$
- 7: **else if** task is regression **then**
- 8: $\hat{y} \leftarrow \frac{1}{k} \sum_{(x_i, y_i) \in \mathcal{N}_k(x)} y_i$
- 9: **end if**
- 10: **return** \hat{y}

As a representative application of KNN, Christodoulou et al. explored its excellence in rainfall prediction based on weather radar measurements, by comparing with a neural network self-organizing map (SOM)Christodoulou et al. [2004]. In 2023, Setya et al. compared Multiple Linear Regression (MLR) and KNN algorithms for monthly rainfall prediction in Semarang, using temperature, humidity, wind speed, wind direction and sunshine duration as predictorsSetya et al. [2023]. Experimental results under two dataset split scenarios (90:10 and 80:20) demonstrate that KNN with a 90:10 split achieved the lowest error values (MAE = 1.22, RMSE = 2.87), outperforming MLR both in accuracy and robustness. The superior performance of KNN can be attributed to its non-parametric characteristic, which allows it to model complex, nonlinear relationships between meteorological variables and rainfall without assuming a specific functional form. Unlike MLR, which relies on linear assumptions and is sensitive to multicollinearity, KNN can flexibly adapt to irregular data patterns and is relatively robust to noisy datasets, provided an appropriate value of K is chosen. Furthermore, its simplicity in implementation and interpretability in terms of 'Nearest Neighbors' make it appealing for operational forecasting, especially when domain experts need intuitive explanations for predictions.

5.5.3 CNN based models

Although ANN models solved the non-linear regression problem in prediction, higher classification accuracy is expected when more image feature is used. Convolutional Neural Network (CNN)Lecun et al. [1998], which possesses the ability to effectively exploit spatial context by incorporating neighborhood pixel information, has attracted the attention of researchers in recent years. In general, a CNN is structured to automatically and adaptively learn spatial hierarchies of features through multiple convolutional layers and pooling layers, combining these with non-linear activation functions and fully connected layers prior to the output. This design makes the network to capture low-level visual patterns in the early stages, progressively abstracts them through successive processing, and integrates them into high-level representations suitable for classification or regression tasks.

As illustrated in Figure 4, the convolution operation in a CNN uses a simple 4×4 input image patch X and a 3×3 kernel. The kernel is sequentially applied to overlap subregions of the input through cross-correlation, where corresponding elements are multiplied and summed to produce a single scalar value. Specifically, the highlighted 3×3 region in the upper-left corner of the input is multiplied elementwise with the kernel, and the products are summed to yield the output at position $Y_{1,1} = 24$. The kernel is then shifted one step to the right, generating the output at $Y_{1,2} = 16$. Repeating this process across the input produces the complete 2×2 feature map. After the convolution step, a pooling operation can be applied to further downsample the resulting feature map. Pooling reduces the spatial resolution while retaining the most salient information, thereby improving computational efficiency and providing a degree of translational invariance. In this case, the pooled output is resized to a single scalar value $\max\{24, 16, 20, 37\} = 37$. Alternatively, average pooling could be used to compute the mean value within each region. Such pooling operations play an important role in progressively summarizing the feature representations learned by the network.

A typical example is a purely CNN-based model using radar composite data from DWD to predict rainfall in GermanyAyzel et al. [2020]. The CNN architecture captures spatial correlations in consecutive radar frames, taking recent radar reflectivity maps as input and directly predicts precipitation fields for future lead times. The evaluation showed that the CNN produced more accurate precipitation predictions than both persistence and optical flow, especially for convective rainfall. Another application is PERSIANN-CNN, proposed by Sadeghi et al.Sadeghi et al. [2019], using a CNN architecture that processes two input channels (IR and WV) through separate convolutional branches. Their model took infrared (IR) channel ($10.7 \mu\text{m}$) and Water Vapor (WV) channel ($6.7 \mu\text{m}$) from Geostationary Operational Environmental Satellite (GOES) as input data, with a rainfall rate map at the same spatial and temporal resolution as the output target. As shown in Figure 5, the inputs were separately convolved in 2 branches in order to extract diverse features, and then were merged with a concatenation function. Prior to the final output, the researchers upsampled the intermediate result by convolutional transpose function (2D ConvTranspose). Another note worth mentioning is they chose rectified linear unit (ReLU) as the activation function for nonlinearity and simplicity in computing the gradient. In the same year, Pan et al. developed a CNN-based approach to improve precipitation estimation by integrating multiple remote sensing productsPan et al. [2019]. Using the IMERG dataset as a reference, the CNN model was trained to correct biases and errors in satellite-derived precipitation estimates by exploiting spatial patterns and multi-source inputs. The results show that the CNN approach significantly outperformed traditional bias-correction methods, achieving lower RMSE and higher correlation coefficients across diverse climatic regions and precipitation regimes. The model demonstrated a strong ability to capture both large-scale precipitation patterns and localized extremes, addressing limitations in conventional retrieval algorithms.

Building on this foundation, Wang et al. introduced the IPEC (infrared precipitation estimation using a convolutional neural network) framework, which expanded the design to a 5-channel CNN using images of multiple GOES IR bands. The IPEC framework emphasizes multispectral feature fusion and cascaded estimation, significantly improving detection skill across diverse U.S. regionsWang et al. [2020]. Later, CNN-based models utilizing IR imagery from FengYun series geostationary meteorological satellite were introduced to estimate different regions' precipitationWang

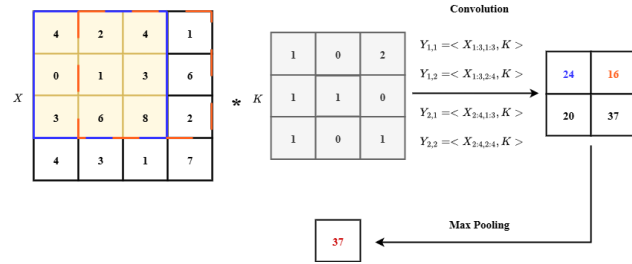


Figure 4: Convolution and Max Pooling.

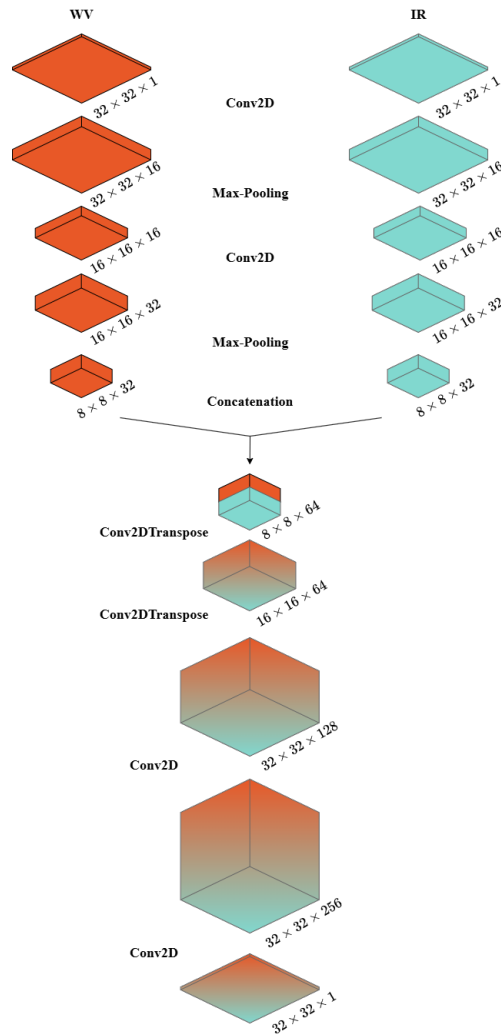


Figure 5: PERSIANN-CNN Model by Sadeghi et al. Sadeghi et al. [2019].

et al. [2021a], Xue et al. [2021]. By extracting spatial features directly from raw satellite data, these models could effectively learn the nonlinear mapping between cloud-top brightness temperature patterns and surface precipitation rates. Experimental evaluations demonstrate that the CNN approaches outperformed traditional statistical regression methods and infrared-based rainfall retrieval algorithms, delivering higher estimation accuracy and improved spatial detail. In parallel, Niu et al. moved beyond instantaneous retrieval to short-term forecasting by integrating radar echoes, temperature fields and precipitation data into a hybrid multi-channel ConvLSTM-3D CNN framework Niu et al. [2020]. Despite differences in scope—regional vs. global, retrieval vs. forecasting—all converge on the conclusion that deep learning surpasses traditional IR-based methods in accuracy, spatial detail, and adaptability. In addition, CNN also has enhanced quantitative precipitation estimation, demonstrating improved accuracy over traditional radar-based methods, particularly in regions with complex terrain Cheng et al. [2023].

5.5.4 SVM based models

As complexity and non-linearity of weather evolution increased, traditional statistical methods shows disadvantages in processing data from various sources. Support Vector Machine (SVM), based on statistical learning and Vapnik-Chervonenkis (VC) dimensional theories Vapnik and Chervonenkis [1971], was initially introduced to solve nonlinear and high dimensional pattern recognition problems Cortes and Vapnik [1995]. SVM is a supervised learning algorithm used primarily for classification (and also regression). The core idea is to find the optimal hyperplane that separates data points from different classes with the maximum margin. The hyperplane is a decision boundary defined as

$$\mathbf{w}^T \mathbf{x} + b = 0$$

where \mathbf{w} is the normal vector and b is the bias. SVM maximizes the margin, which represents the distance between the hyperplane and the closest data points (called support vectors). Specifically, to implicitly map data into high-dimensional space without computing it directly, known as the kernel trick, a kernel function $K(x_i, x_j)$ is used, named Dual Problem of SVM. Dual Problem has a form

$$\begin{aligned} \max_{\alpha} & \sum_{i=1}^N \alpha_i - \frac{1}{2} \sum_{i,j=1}^N \alpha_i \alpha_j y_i y_j K(x_i, x_j) \\ \text{subject to} & \quad 0 \leq \alpha_i \leq C, \quad \sum_{i=1}^N \alpha_i y_i = 0 \end{aligned}$$

where α_i and α_j are Lagrange multipliers associated with the training samples (x_i, y_i) and (x_j, y_j) , respectively. C controls the trade-off between margin width and classification error. Then, SVM takes a decision function to predict the class of an input sample \mathbf{x} , denoted as $f(\mathbf{x}) = \text{sign}(\sum_{i=1}^N \alpha_i y_i K(\mathbf{x}_i, \mathbf{x}))$. In recent years, the frontier of weather prediction has developed a series of models based on SVM for its ability to extract information from historical data and better performance in consistency compared with ANN Hong [2008]. Lu et al. applied SVM to predict monthly rainfall in a region of China with different kernel functions Lu and Wang [2011]. Yin et al. combined SVM regression with quantile-based bias correction techniques (Quantile Mapping and CDF-transform) to enhance real-time hourly precipitation forecasts in Japan Yin et al. [2022]. This combined method outperforms other approaches by leveraging the strengths of both components: SVM's spatial modeling and CDF-transform's distributional correction. It has achieved higher correlation, lower bias, and better detection of extreme events, particularly during wet months like July. The researchers also applied an SVM-CDF approach to improve global subseasonal to seasonal (S2S) precipitation forecasts using ECMWF data on a daily scale Yin et al. [2023], demonstrating this approach scales well globally for longer-range forecasts. However, their approaches face common limitations in handling dry or extreme conditions, highlighting areas for future improvement, such as better data balance or integration of physical indices. To tackle both non-linearity and non-stationarity, Rezaiy et al. presented a novel hybrid model that integrates Ensemble Empirical Mode Decomposition (EEMD) with Support Vector Machine (SVM) to enhance drought forecasting accuracy, using the Standardized Precipitation Index (SPI) as a drought indicator Rezaiy and Shabri [2024]. In the following year, the authors proposed a hybrid Wavelet-Support Vector Machine (W-SVM) model to enhance the accuracy of drought forecasting based on the Standardized Precipitation Index (SPI). By combining Discrete Wavelet Transform (DWT) with SVM, the model effectively decomposes SPI time series into multiple components, then, then, predicts individually and reconstructs Rezaiy and Shabri [2025].

5.5.5 RNN and LSTM based models

As shown in Figure 5, a Recurrent Neural Network (RNN) is a class of artificial neural networks designed to process sequential data by maintaining a hidden state that captures information from previous time steps. Unlike feedforward networks, RNNs incorporate recurrent connections, enabling the transfer of information forward in time, which makes

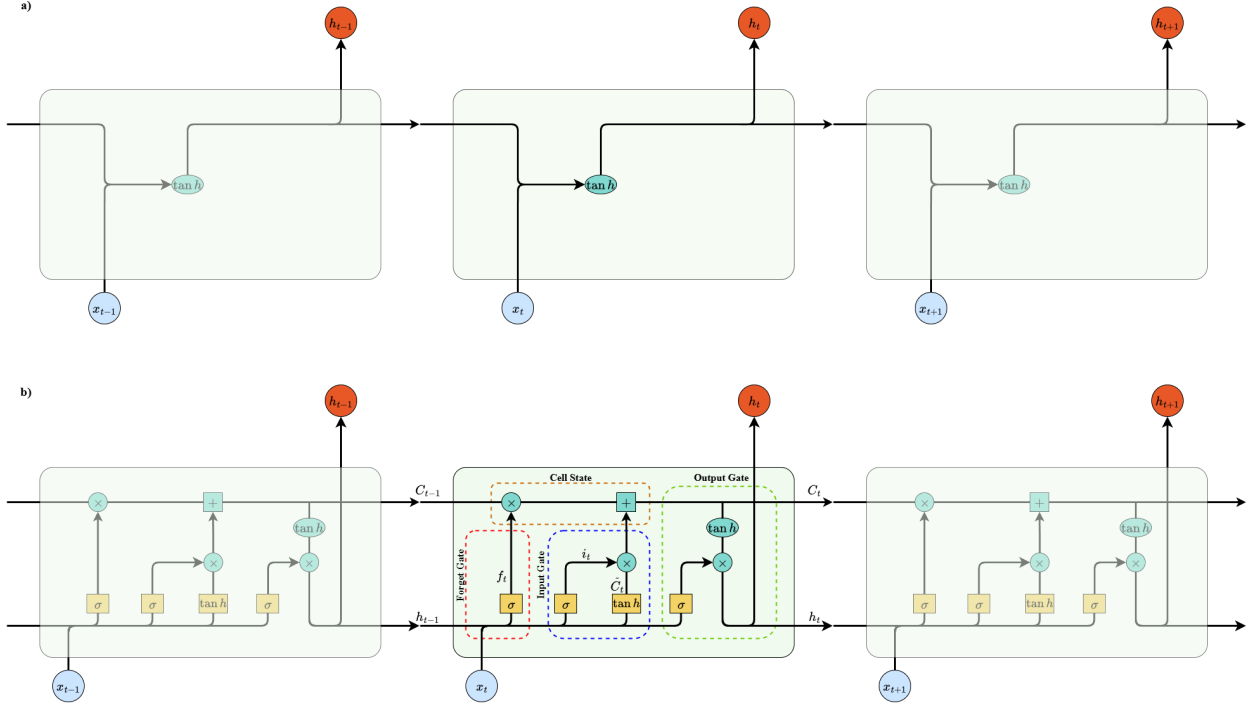


Figure 6: RNN and LSTM model. a) RNN model. b) LSTM model. Fang et al. [2021]

them well-suited for tasks where the order of inputs is important, such as time series forecasting, speech recognition, natural language processing, and meteorological prediction Elman [1990], Goodfellow et al. [2016].

Mathematically, at each time step t , the hidden state h_t is updated according to

$$h_t = f(W_x x_t + W_h h_{t-1} + b),$$

where W_x and W_h are weight matrices, b is a bias term, and f is a nonlinear activation function (e.g., tanh or ReLU).

Relying on the power of RNN, some innovative approaches have been introduced to precipitation prediction. Ma et al. proposed Multimodal RNN (MM-RNN) that fuses multiple meteorological data streams—such as radar reflectivity, ground-based meteorological station data, and atmospheric reanalysis variables—into its predictive framework Ma et al. [2023]. This model employs three modules—meteorological elements’ prediction module (EM), radar prediction module (RM), and modal fusion module (MFM). EM and RM apply RNN structures to capture their unique temporal dynamics, while MFM combines the hidden states from all modalities before the final output layer, allowing the network to learn complementary relationships between atmospheric variables. By training and evaluating with MeteoNet and RAIN-F datasets, the multimodal architecture shows better performance across most metrics compared with other unimodal RNN models.

While RNNs are capable of modeling temporal dependencies, standard RNNs encounter difficulties with long-term dependencies due to the vanishing or exploding gradient problem. This limitation has motivated the development of advanced variants such as Long Short-Term Memory (LSTM) networks Hochreiter and Schmidhuber [1997], which use gating mechanisms to selectively retain or discard information, thereby enabling the modeling of longer-range dependencies more effectively. A standard RNN only have a simple repeating component, such as a tanh layer. In contrast, the corresponding component in LSTM has 4 neural network layers, namely, 3 sigmoid layers and a tanh layer. In detail, the unique structure in LSTM is called gate Gers et al. [1999], which consists of a sigmoid layer and a pointwise operation. The first gate, called the “forget gate,” decides what to throw away from the old cell state.

$$f_t = \sigma(w_f \cdot [h_{t-1}, x_t] + b_f).$$

Where σ represents a sigmoid function that controls the proportion of remaining information according to h_{t-1} and x_t . 0 means totally ignore, while 1 means keeping.

Then, choose information from the current cell state for storing.

$$i_t = \sigma(w_i \cdot [h_{t-1}, x_t] + b_i).$$

$$\tilde{C}_t = \tanh(w_c \cdot [h_{t-1}, x_t] + b_c).$$

Where i_t decides what values need to be updated according to the current input, followed by a vector of candidate values \tilde{C}_t .

The next step is to combine them together. Multiply the values inherited from the older state C_{t-1} , and the things that we want to forget earlier, then add $i_t * \tilde{C}_t$.

$$C_t = f_t * C_{t-1} + i_t * \tilde{C}_t$$

Finally, the output h_t is decided by a filtered operation of the current state and the result of a sigmoid layer.

$$o_t = \sigma(w_o \cdot [h_{t-1}, x_t] + b_o)$$

$$h_t = o_t * \tanh(C_t)$$

Building on such recurrent architectures, researchers have sought ways to extend their capabilities to handle both spatial and temporal dependencies simultaneously. In 2015, Shi et al. proposed a pioneering model named Convolutional LSTM (ConvLSTM), specifically designed for spatio-temporal sequence forecasting tasks like precipitation nowcasting Shi et al. [2015]. This model extends traditional fully connected LSTM (FC-LSTM) by integrating convolutional operations into both the input-to-state and state-to-state transitions, and the results show that it outperforms the state-of-the-art ROVER algorithm and FC-LSTM models in several key ratios (e.g., MSE, CSI, FAR, POD, Corr.). Years later, baseline models, Trajectory Gated Recurrent Unit (TrajGRU) Shi et al. [2017] and PredRNN Wang et al. [2017] were developed as an extension of ConvLSTM to address its limitations in modeling non-stationary and location-variant spatio-temporal dynamics. Whereas ConvLSTM applies fixed convolutional kernels for state transitions across spatial grids, TrajGRU learns location-variant recurrent connections through dynamically generated flow fields. Ignited by these groundbreaking studies, PredRNN++ Wang et al. [2018] was soon proposed to refine the architecture with Causal LSTMs and a more effective spatio-temporal memory trajectory design. Unlike ConvLSTM's fixed convolutional recurrence and TrajGRU's learned but localized trajectories, PredRNN++ emphasized long-term dependency modeling through a flexible memory passing scheme across layers and time steps. To demonstrate the strength of PredRNN++, Bonnet et al. applied this model to nowcast the precipitation in São Paulo with weather radar images Bonnet et al. [2020]. The model shows significant improvement above the conventional precipitation nowcasting model across multiple lead times. Luo et al. also proposed PFST-LSTM, which extended ConvLSTM with a pseudoflow prediction mechanism to explicitly account for the motion of precipitation systems Luo et al. [2021]. Compared with Shi et al.'s original ConvLSTM, PFST-LSTM showed enhanced stability and accuracy, particularly in forecasting complex storm dynamics and longer lead times.

To explore potential applicabilities of LSTM in lightweight models, Pathan et al. proposed an efficient LSTM-based framework for forecasting precipitation using historical rainfall observations Pathan et al. [2021]. The model was trained and evaluated on monthly precipitation data from 1990 to 2020 collected at the Alpena Regional Airport, Michigan, U.S., obtained from the NOAA Climate Data Online service. To enhance data quality and improve predictive stability, a Box-Cox transformation was applied, reducing skewness and approaching normal distribution in the rainfall time series. The designed LSTM network comprises only two recurrent layers and approximately 13000 trainable parameters, which significantly reduces computational cost while maintaining competitive accuracy. This makes the model well-suited for rapid training and efficient forecasting in practical scenarios. Furthermore, to insightfully exhibit the potential of ConvLSTM in precipitation prediction, Gamboa-Villafruela et al. proposed a Contextual Self-Attention Convolutional LSTM (CSA-ConvLSTM) framework for precipitation nowcasting, integrating convolutional recurrence with an attention mechanism to better capture spatial dependencies and temporal context Gamboa-Villafruela et al. [2021]. Unlike standard ConvLSTM, which treats all features equally within local receptive fields, CSA-ConvLSTM introduces a contextual self-attention module that adaptively assigns weights to spatial regions and temporal frames. This special design allows the model to focus more on dynamically relevant areas of radar echoes, such as convective storm centers, while suppressing less informative background patterns. The model was trained and validated on radar echo datasets, and experimental comparisons demonstrated that CSA-ConvLSTM outperformed baseline models, including ConvLSTM, TrajGRU and standard attention-augmented ConvLSTM variants. It achieved more accurate short-term forecasts, with sharper structural preservation and reduced error accumulation across lead times. The integration of self-attention mechanism not only enhanced predictive skill but also improved interpretability, providing insight into which spatial-temporal regions influenced forecasts the most. Moreover, Shen et al. constructed a CEEMDAN-SVM-LSTM model to forecast monthly precipitation in Lanzhou City, combining CEEMDAN (fully adaptive noise ensemble empirical modal decomposition algorithm), SVM and LSTM algorithms together Shen and Ban [2023]. They

compared separately LSTM with other baseline models, and found LSTM outperformed in several evaluation metrics like RMSE, MSE, and MAE. To demonstrate the effect of CEEMDAN module, they compared CEEMDAN-LSTM and CEEMDAN-SVM with single LSTM and SVM, respectively, and the result met the expectations. Finally, the combined CEEMDAN-SVM-LSTM model, showed better prediction ability than the CEEMDAN-LSTM model, with a 57.5% improvement in RMSE, a 55.1% improvement in MAE, and 33.8% progress in R^2 index.

Extending this idea, more hybrid models have been developed to enhance LSTM's predictive capability under non-stationary and highly variable rainfall conditions. The Wavelet-ARIMA-LSTM model combines wavelet decomposition for denoising, ARIMA (autoregressive integrated moving average) for linear dynamics and LSTM for nonlinear learning, resulting in improved robustness across multiple meteorological stations Wu et al. [2021]. Similarly, the CEEMD-LSTM model utilizes complementary ensemble empirical modal decomposition (CEEMD) to break down rainfall signals into intrinsic components before applying LSTM, thereby improving accuracy and stability in capturing not only short-term fluctuations but also long-term patterns Zhang et al. [2021a]. These hybrid approaches highlight the significance of temporal decomposition and hybridization for improving forecasts from historical rainfall series, as well as illustrate how deep learning has advanced both the spatial modeling of storm evolution and the temporal prediction of rainfall variability, offering a more comprehensive toolkit for precipitation forecasting.

5.5.6 GNN based models

To capture and learn from the irregular topology and relational dependencies inherent in graph-structured data, a novel class of model named graph neural networks (GNN) has been developed. Basically, a graph G consists of a set of nodes V and edges E , where each node can represent an entity and each edge represents a relationship or interaction between entities. The target of GNN is to learn a state embedding $h_v \in \mathbb{R}^s$ for each node, which includes features in node itself and relationship of its neighborhood, defined as

$$h_v = f(x_v, x_{e[v]}, h_{\mathcal{N}v}, x_{\mathcal{N}v})$$

where x_v , $x_{e[v]}$, $h_{\mathcal{N}v}$, $x_{\mathcal{N}v}$ are the features of v , the features of its edges, the states and the features of the neighbored nodes, respectively. f here is a parametric function named the local transition function. An output o_v could be produced by h_v and features x_v by a local output function g , denoted as

$$o_v = g(h_v, x_v)$$

In general, f and g can be interpreted as feedforward neural networks. All features and all states can be stacked in matrices \mathbf{X} and \mathbf{H} , respectively, and a global transition function F stacks all versions of f for all nodes Zhou et al. [2020]. To train \mathbf{H} , an iterative scheme denoted as

$$\mathbf{H}^{t+1} = F(\mathbf{H}^t, \mathbf{X})$$

where t is the t -th iteration step.

Nevertheless, traditional GNN-based approaches often overlook the integration of rich semantic features available from high-resolution satellite imagery. To overcome this limitation, recent works have introduced hybrid graph neural frameworks that explicitly combine physical drivers and radar-derived semantics. For example, Chen et al. proposed a physics-informed GNN for precipitation forecasting over China, using the ERA5 reanalysis dataset and Chinese meteorological observations Chen et al. [2024]. In their model, each graph node corresponded to a geographical grid cell containing multiple atmospheric predictors, including vertical velocity, relative humidity, geopotential height and temperature fields, while edges encoded spatial and temporal correlations. The architecture combined graph convolutional layers for neighborhood aggregation with temporal gated units to capture evolving rainfall dynamics. To enhance physical consistency, they embedded large-scale circulation indices (e.g., ENSO-related patterns) directly into the graph structure. Evaluation was performed using metrics such as Root Mean Square Error (RMSE), Critical Success Index (CSI) and Probability of Detection (POD), with results showing significant gains over CNN, ConvLSTM and Transformer baselines, particularly in reproducing extreme precipitation events and maintaining regional rainfall variability. In contrast, Peng et al. introduced the CNGAT (Convolutional Node Graph Attention Network) for radar-based quantitative precipitation estimation (QPE) Peng et al. [2022b]. The study used China's operational weather radar network, which provides high-resolution radar reflectivity data. In this model, radar pixels were treated as graph nodes, with convolutional modules first extracting local radar echo features. Then, features of these nodes were passed through a multi-head graph attention mechanism, which dynamically weighted the spatial dependencies among radar pixels to capture the irregular and evolving structure of precipitation cells. Benchmarks included traditional Z-R relationships, CNN-based QPE models and ConvLSTM architectures, evaluated on standard QPE metrics such as Correlation Coefficient (CC), Normalized Mean Bias (NMB) and RMSE. CNGAT consistently outperformed baselines, showing marked improvements in rain-rate accuracy and in capturing the fine-scale spatial distribution of rainfall.

During the last few years, some innovative models have been integrated with GNNs. PN-HGNN, a novel precipitation nowcasting framework that combines a spatio-temporal attention mechanism with hypergraph convolution layers, was

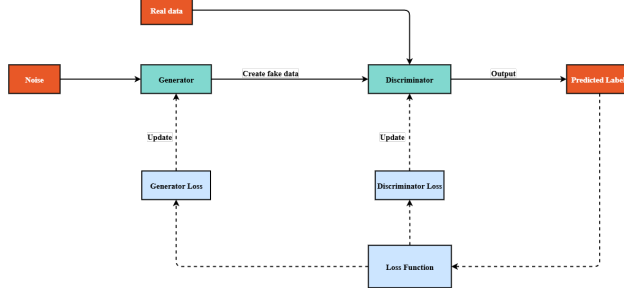


Figure 7: GAN ArchitecturePachika et al. [2024]

proposed to process spatial dependencies and temporal progression across multiple radar framesSun et al. [2024]. Peng et al. introduced a multilevel rainfall forecasting framework based on structured GNNPeng et al. [2023]. This framework was separated into multiple submodels, which were trained for different rainfall thresholds (e.g., 0.1 mm, 3 mm, 10 mm, 20 mm). Each submodel utilizes the graph neural network architecture to propagate information spatially and temporally. Across all rainfall levels, the proposed model consistently outperformed ECMWF’s IFS (integrated forecasting system) in Threat Score (TS) and Heidke Skill Score (HSS), particularly at higher intensities. The result shows that the framework can serve as a post-processing enhancement for operational forecasts rather than a replacement of NWP, offering a computationally efficient route to improve rainfall prediction in real-world applications. Inspired by this research, Yousaf et al. designed a hybrid GNN-based framework to post-process and enhance local-scale numerical weather forecasts in the Calabria region of ItalyYousaf et al. [2025]. The proposed spatio-temporal GNN with six graph convolution layers and ReLU activations was trained using MSE loss, and it provided tangible improvements over classical WRF (Weather Research Forecasting) outputs and other ML post-processors. Pham et al. employed the encoder-decoder paradigm, specifically, they used GNNs as an encoder and CNNs as a decoder, which interprets high-dimensional spatial-temporal information into a low-dimensional format and extracts features to produce the final precipitation estimation, respectivelyPham et al. [2024]. Another famous GNN-based model, namely GraphCast, was developed by Google DeepMind Research, designed with an encoder-processor-decoder architectureLam et al. [2023]. The encoder, processor, and decoder formed a coherent graph-based pipeline in which the encoder projected atmospheric variables onto a high-resolution multimesh representation, the processor performed hierarchical message passing to capture global spatial dependencies, and the decoder reconstructed the updated atmospheric state on the latitude-longitude grid as a normalized residual correction to the previous forecast step. Although the model has 36.7 million parameters, it achieved superior performance over the most accurate operational deterministic systems (ECMWF’s HRES) on approximately 90% of 1380 verification targets, demonstrating improved forecast skill across multiple atmospheric variables and lead times up to 10 days. To evaluate the ability of GraphCast’s precipitation prediction, Yan et al. validated the model against 2393 ground observation stations in mainland ChinaYan et al. [2025]. The result shows that GraphCast maintained forecast stability across increasing lead times, compared with ECMWF’s forecasts in multiple metrics (e.g., CC, ME, RMSE, POD). These studies highlight how next-generation GNNs leverage both physics-informed inputs and radar-derived semantics to overcome the limitations of earlier graph-based approaches. By grounding graph nodes in real atmospheric variables and enabling attention-based, non-local feature interactions, these models advance precipitation prediction toward higher accuracy, better generalization and improved interpretability.

5.5.7 GAN based models

Generative Adversarial Networks (GANs), introduced by Goodfellow et al.Goodfellow et al. [2014], are a class of generative models that learn to synthesize realistic data through an adversarial training process between two neural networks: a Generator G and a Discriminator D . As shown in Figure 7, the generator aims to produce data samples that mimic the real data distribution, while the discriminator attempts to distinguish between real and generated samples. This interaction can be formulated as a minimax optimization problem:

$$\min_G \max_D \mathbb{E}_{x \sim p_{\text{data}}(x)} [\log D(x)] + \mathbb{E}_{z \sim p_z(z)} [\log (1 - D(G(z)))]$$

Where $p_{\text{data}}(x)$ is the real data distribution and $p_z(z)$ is the prior distribution of the generator’s input noise vector z . So, in an adversarial training loop, G and D are trained alternately, G improves to fool D , and D improves to detect fake data.

In precipitation forecasting, GANs are often implemented in a conditional form (cGANs), where the generator is conditioned on input meteorological fields to produce future precipitation maps. It’s an extension of the original GAN, but instead of generating samples purely from random noise, the generation process is conditioned on some extra

information. The formulation is denoted as:

$$\begin{aligned} & \min_G \max_D \mathbb{E}_{x \sim p_{\text{data}}(x)} [\log D(x|y)] \\ & + \mathbb{E}_{z \sim p_z(z)} [\log (1 - D(G(z|y)))] \end{aligned}$$

Where y is a condition. As an exemplary application, Hayatbini et al. trained a cGAN with MSE loss to learn the complex distribution of precipitation from the satellite imageries Hayatbini et al. [2019]. Wang et al. also introduced PrecipGAN, a novel deep learning framework that utilizes a cGAN to produce highly accurate, high-resolution satellite precipitation estimates Wang et al. [2021b]. The model is trained on a multi-sensor dataset that includes both microwave and infrared data, for outputting a high-resolution (1 km) daily precipitation estimate with low latency.

Xu et al. proposed Two-Stage UA-GAN, a deep learning framework for precipitation nowcasting using radar echo map extrapolation Xu et al. [2022]. The model takes a Trajectory Gated Recurrent Unit (TrajGRU) network in stage 1 for pre-prediction, capturing large-scale motion patterns effectively, but produces blurred outputs. In stage 2, a U-Net-based Generative Adversarial Network (UA-GAN) enhanced with a 2-dimensional stacked residual attention block (2DSRAB) refines Stage 1 outputs. The model takes HKO-7 radar echo dataset (2009–2015) from the Hong Kong Observatory as input, with predicted radar echo frames for the next hour (10 frames) at high spatio-temporal resolution as output. UA-GAN achieved the lowest RMSE (0.099), the highest SSIM (0.585), and markedly better CSI and HSS across all thresholds compared to optical-flow (ROVER) and deep learning baselines (ConvLSTM, ConvGRU, TrajGRU, PredRNN++).

5.5.8 Transformer based models

Recurrent Neural Networks (RNNs) and their gated variants, such as Long Short-Term Memory (LSTM), have historically been the backbone of sequence modeling tasks due to their ability to capture temporal dependencies through sequential processing. However, as the significant growth in data size of input, these models suffer from inherent limitations, including difficulty modeling long-range dependencies, limited parallelization during training, and gradient vanishing or exploding issues. A neural network architecture based on self-attention mechanisms was introduced to enable large-scale parallelism and scalability, namely Transformer Vaswani et al. [2017]. The Transformer architecture is a deep learning model designed to process sequential data without relying on recurrence. Instead, it leverages a self-attention mechanism to model dependencies between sequence elements, allowing all tokens to be processed in parallel Aleissaee et al. [2023]. This innovation greatly improves training efficiency and the ability to capture long-range dependencies compared to traditional recurrent neural networks. Refer to Figure 8, a Transformer consists of two primary components: the encoder and the decoder. The encoder transforms the input sequence into a contextual representation through stacked layers of multi-head self-attention and position-wise feed-forward networks, each followed by residual connections and layer normalization. The decoder generates the output sequence autoregressively, using masked multi-head self-attention to prevent access to future positions, cross-attention to incorporate encoder outputs, and feed-forward layers for transformation. The core of Transformer is the attention mechanism, which is a method for dynamically focusing on the most relevant parts of the input when producing each output. Mathematically, in standard attention:

$$\text{Attention}(Q, K, V) = \text{softmax}\left(\frac{QK^T}{\sqrt{d_k}}\right)V$$

Where Q represents for queries, K represents for keys, V represents for values, d_k is the dimensionality of the key vectors. For spatio-temporal meteorological data, precipitation at a given grid cell may depend heavily on patterns far away (e.g., an incoming storm). Attention enables the model to dynamically capture both local and long-range dependencies without fixed kernel sizes or recurrence.

Based on the power of Transformer, a novel spatio-temporal SwinUNet3D model was proposed for short-term weather forecasting, leveraging the 3D Swin-transformer in a U-net architecture to predict 8 hours ahead weather events from hourly gridded data Bojesomo et al. [2021]. By replacing all convolutional layers in the traditional U-Net with 3D Swin Transformer blocks, the model outperforms traditional U-Net and persistence baselines in the core and transfer tasks of the IEEE Big Data Weather4cast Competition. As Transformer unfolded competitive accuracy and computational efficiency, more and more projects harnessed it to address weather forecasting tasks. Earthformer, a novel space-time Transformer model designed for Earth system forecasting Gao et al. [2022a]. The model is built on a custom Cuboid Attention mechanism that dramatically reduces the computational cost of self-attention in high-dimensional spatio-temporal data. Earthformer achieves state-of-the-art performance across real-world precipitation nowcasting (SEVIR dataset) and long-term sea surface temperature forecasting (ICAR-ENSO dataset). Another model, named Preformer, is a lightweight transformer-based framework specifically designed for precipitation nowcasting, adopts a minimalist encoder-translator-decoder architecture with only two Transformer layers, outperforms both traditional and modern baselines (e.g., ConvLSTM, SimVP, TAU, gSTA) on ERA5 and WeatherBench datasets Jin et al. [2024].

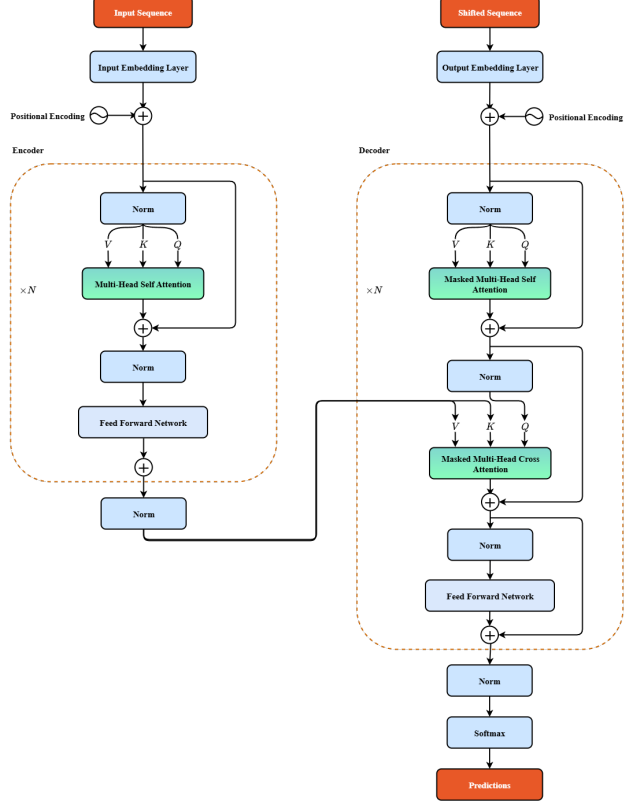


Figure 8: Transformer Architecture Vaswani et al. [2017], Aleissaee et al. [2023]

Similarly, the recently proposed SwinNowcast model also demonstrates the potential of transformer-based architectures for precipitation nowcasting Li et al. [2025a]. Built upon the Swin Transformer’s hierarchical representation learning and shifted window attention, SwinNowcast captures both local and global spatio-temporal dependencies in radar echo sequences. Extensive evaluations on benchmark datasets indicate that it surpasses leading baselines, including ConvLSTM and PredRNN, in predictive accuracy and the visual realism of forecasted precipitation maps. Multi-Scale Spatial-Temporal Transformer (MSTT) Li et al. [2025b], a model for meteorological variable forecasting, especially well-suited for precipitation prediction, addressing the challenge of capturing both global and local dependencies in spatio-temporal climate data.

Additionally, Li et al. expanded Transformer to Quantitative Precipitation Nowcasting (QPN) Li et al. [2023a], which aims to predict short-term, high-resolution precipitation fields based on recent radar echo observations, formulated as below.

$$\hat{X}_{t+1}, \dots, \hat{X}_{t+m} = \operatorname{argmax}_{X_{t+1}, \dots, X_{t+m}} p(X_{t+1}, \dots, X_{t+m} | X_{t-n}, X_{t-3}, \dots, X_t)$$

Where X_i is the actual frame at time i , and \hat{X}_j is the predicted frame at time j . m and n are the amount of input frames and predicted frames respectively. The proposed LPT-QPN architecture leverages a Transformer backbone augmented with physics-informed attention, where the standard self-attention mechanism is constrained by the advection equation, a fundamental physical law describing the motion of precipitation fields. Specifically, what is obviously different from previous researchers, the authors introduced a new attention mechanism named Multihead Squared Attention (MHSAs)

in order to reduce the computational complexity of the QPN task.

$$\begin{aligned}
\hat{\mathbf{X}} &= W_1 \cdot \text{reshape} \left(\text{Attention} \left(\hat{\mathbf{Q}}, \hat{\mathbf{K}}, \hat{\mathbf{V}} \right) \right) + \mathbf{X}, \\
\text{Attention} \left(\hat{\mathbf{Q}}, \hat{\mathbf{K}}, \hat{\mathbf{V}} \right) &= \text{Sigmoid} \left(\hat{\mathbf{Q}} \cdot \hat{\mathbf{K}}^T / \alpha \right) \cdot \hat{\mathbf{V}}, \\
\hat{\mathbf{Q}} &= \text{reshape} \left(W_1^Q W_3^Q \mathbf{X}_{LN} \right), \\
\hat{\mathbf{K}} &= \text{reshape} \left(W_1^K W_3^K \mathbf{X}_{LN} \right), \\
\hat{\mathbf{V}} &= \text{reshape} \left(W_1^V W_3^V \mathbf{X}_{LN} \right), \\
\hat{\mathbf{Q}}, \hat{\mathbf{K}}, \hat{\mathbf{V}} &\in \mathbb{R}^{C \times H \times W}, \mathbf{X} \in \mathbb{R}^{C \times H \times W}
\end{aligned}$$

Where, \hat{Q} , \hat{K} , \hat{V} are the query, key and value matrices reshaped from feature maps of previous 1×1 point-wise convolutions and 3×3 depth-wise convolutions, i.e. $W_1^{(\cdot)}$, $W_3^{(\cdot)}$. X_{LN} is the layer normalized input tensor and α is the trainable parameter. Here, a sigmoid activation function instead of softmax was applied to make the computation process more suitable for feature maps of precipitation data, because the sum of attention weights is not necessarily equal to 1. Comparative experiments on benchmark radar datasets demonstrate that LPT-QPN achieves state-of-the-art or near state-of-the-art performance while using fewer parameters and computational resources than deep recurrent models (e.g., ConvLSTM, PredRNN) and purely data-driven Transformers (e.g., Swin Transformer, SimVP). The model particularly excels in preserving fine-scale precipitation structures and reducing displacement errors over longer lead times.

As an emerging structure in machine learning, there are more and more transformer-based models applied in precipitation prediction in recent years. For example, Piran et al. applied a transformer generative framework for precipitation nowcasting to the Soyang Dam basin in South Korea, demonstrating superior performance compared to default models (cGANs, ConvLSTMs, U-Net and pySTEP), as validated through multiple verification metrics including PCC, RMSE, NSE, CSI and FSSPiran et al. [2024]. Zhao et al. presented a spatio-temporal transformer-based denoising diffusion model designed to advance the realism and physical consistency of precipitation nowcastingZhao et al. [2024a]. They experimented with the SEVIR dataset and finally found that the proposed approach yielded visually sharper, more realistic forecasts and achieved competitive meteorological evaluation scores across a range of rainfall intensities. Li et al. introduced a diffusion transformer framework with causal attention for high-resolution precipitation nowcasting, taking advantage of causal attention to ensure strict temporal ordering and directional information flowLi et al. [2024a]. UTrans-Net, a U-shaped neural architecture integrating transformer attention mechanisms, was proposed by Cao et al. in 2022Cao et al. [2022]. The neural architecture was evaluated on the China Meteorological Administration dataset, and the result highlighted the model's strong generalization ability and suitability for real-time forecasting applications. MDTNet, namely multiscale deformable transformer network, uses Deformable Multi-Head Self-Attention (D-MHSA), allowing spatially adaptive attention to strong precipitation regionsZhao et al. [2024b]. Particularly, the researchers novelly introduced Fourier space regularization and adversarial losses that constrain the model to reproduce high-frequency spectral components. Dong et al. presented a transformer-based framework designed to enhance radar echo extrapolation by unifying global-local spatiotemporal aggregation with motion-aware learningDong et al. [2022]. HTLA, Hierarchical Transformer With Lightweight Attention, was proposed to efficiently nowcast precipitation based on the KNMI (Koninklijk Nederlands Meteorologisch Instituut) radar dataset, highlighted by Cross-Channel Self-Attention (CSA), Dual Feedforward Network (DFN) and Gaussian Pooling Skip-Connection strategyLi et al. [2024b]. PFformer, a transformer-based model tailored for short-term precipitation forecasting in northern Xinjiang, China, introduces a piecewise-attention Transformer architecture for efficient short-term rainfall predictionXu et al. [2024]. The core innovation of this study lies in replacing the point-wise dot product self-attention of iTransformer with a Segment Correlation Attention (SCAttention) mechanism. This modification reduces computational complexity from $O(L^2)$ to $O(L^2/L_{seg})$ (L and L_{seg} are the length of the time series and the divided length by multiple segments, respectively) by computing correlations between temporal segments rather than individual time steps. LLMDiff, a diffusion model using frozen LLM (large language model) Transformers, was built on Earthformer but extended it into a diffusion-based probabilistic settingShe et al. [2024]. Bi et al. proposed a novel deep generative framework, combining a Vector Quantized Generative Adversarial Network (VQGAN) and an autoregressive Transformer to produce radar-based precipitation forecastsBi et al. [2023b]. The model introduces an Extreme Value Loss (EVL) function derived from Extreme Value Theory (EVT) to model rare, high-intensity rainfall events. Liu et al. applied a model named Multi-Level Transformer Fusion (MLTF) to quantitative precipitation estimation in the source region of the Yellow River basin (SRYRB), which is a sparsely-gauged areaLiu et al. [2024].

6 Existing problems and future directions

6.1 Existing problems

Over the past two decades, neural network architectures—including convolutional neural networks (CNNs), recurrent neural networks (RNNs), attention-based transformers, graph neural networks (GNNs) and hybrid frameworks—have driven significant advances in precipitation prediction across nowcasting, short-range and seasonal-to-interannual (S2S) forecasting. These developments represent a major leap forward from early empirical techniques and classical numerical weather prediction (NWP) systems, offering improved accuracy, adaptability and scalability. To provide clarity, we outline the most pressing issues below, highlighting the key barriers that must be addressed for reliable, scalable and interpretable precipitation prediction.

6.1.1 Generalization beyond the training domain

Neural networks often perform well in regions with dense observations or high climate predictability, but their skill can degrade sharply in data-sparse or teleconnection-weak areas. This challenge is amplified when applying models trained in one climatic regime to another with distinct precipitation drivers.

6.1.2 Data scarcity for long-lead forecasting

Unlike sub-hourly or daily weather datasets, seasonal and S2S precipitation records are short and coarse in temporal resolution. Deep neural networks, with millions of parameters, can be data-hungry and thus prone to overfitting when trained on such limited datasets.

6.1.3 Interpretability challenges

While post-hoc explanation methods (e.g., saliency maps, SHAP values) and built-in mechanisms (e.g., attention layers, variable selection networks) can offer insights into model decision-making, they typically describe statistical associations rather than causal mechanisms. Moreover, interpretability may vary with data splits, raising concerns for operational trust.

6.1.4 Representation of extremes

Many models underpredict rare precipitation extremes. Standard loss functions such as MSE or CRPS prioritize mean accuracy, inadvertently reducing sensitivity to extreme events that are critical for disaster risk management.

6.1.5 Trade-off between complexity and operational feasibility

High-capacity models (e.g., transformers, deep GNNs) can capture complex spatio-temporal dependencies but often require substantial computational resources for training and inference, limiting their practicality for real-time operations in resource-constrained settings.

6.2 Future Directions

While current neural network models have advanced precipitation prediction across multiple scales, future progress will require bridging methodological innovation with practical implementation. The primary trends is hybrid architectures being widely used in precipitation prediction tasks, for they can enhance models' abilities in extracting spatio-temporal information from different resources, and combining physical process knowledge with neural network flexibility can improve both skill and interpretability. For instance, the CSA-ConvLSTM framework Xiong et al. [2021] integrates an attention mechanism to better capture spatial-temporal context. MLSTM-AM Tao et al. [2021], which combines ATWT, LSTM and attention mechanism to optimize the whole prediction structure, showing more skillful than any single component in this structure. Ebtehaj and Bonakdari Ebtehaj and Bonakdari [2024] demonstrated that CNNs offer efficiency and precision in short-term heavy rainfall forecasting, whereas LSTMs achieve superior accuracy for longer lead times and moderate precipitation events. These findings suggest that hybrid frameworks—leveraging CNNs for rapid feature extraction and LSTMs for sequence dependency modeling—could yield more robust and operationally viable solutions for real-time flood forecasting and precipitation nowcasting. The TelNet model Pinheiro and Ouarda [2025] exemplifies this by using a sequence-to-sequence architecture with a variable selection network to provide instance- and lead-wise feature importance for seasonal precipitation forecasting. Its design demonstrates how interpretable modules can be embedded into modern architectures to enhance trustworthiness while maintaining high predictive performance. In a complementary direction, the Rainformer model Bai et al. [2022] illustrates how hybrid

architectural principles can also be applied to improve the balance between different feature types in high-resolution nowcasting. Although Rainformer is primarily designed for accuracy rather than interpretability, its modular structure provides a pathway for embedding interpretable elements, such as attention weight visualization or scale-wise feature attribution, into future hybrid systems. The emergence of physics-guided and interpretable hybrids suggests a trajectory toward architectures that balance predictive skill, physical consistency and transparency.

In this review, related papers published within 3 years (2022-2025) are also supplemented in Table 2 to demonstrate emerging trends toward greater integration of physical knowledge, enhanced data utilization and model interpretability. Other key directions include:

6.2.1 Region-agnostic and transfer learning approaches

Future research should focus on models that generalize across climate regimes via transfer learning, domain adaptation, or pretraining on global climate datasets followed by targeted fine-tuning.

6.2.2 Extreme-event-focused optimization

Loss functions and post-processing methods specifically tailored for extremes (e.g., weighted CRPS, quantile loss, or EVT-based approaches) should be integrated to improve rare-event skill without sacrificing overall accuracy.

6.2.3 Multi-modal and physics-informed integration

Incorporating heterogeneous data sources—such as radar, satellite imagery, reanalysis and climate indices—with physics-informed neural networks (PINNs) or hybrid dynamical-statistical frameworks may yield models that are both skillful and physically consistent.

6.2.4 Spatial scalability and adaptability

Approaches like patch embedding, hierarchical graph structures and adaptive resolution schemes can enable neural networks to handle diverse and large spatial domains without loss of accuracy or interpretability.

6.2.5 Comprehensive benchmarking

To ensure robustness and fairness in evaluation, future studies should benchmark models across multiple climate regimes, lead times and precipitation regimes, moving beyond single-region case studies.

Appendix 1: List of Abbreviations

CBAM: convolutional block attention module

DWD: German Weather Service

FCTH: Hydraulic Technology Center Foundation (Portuguese acronym)

GPM: Global Precipitation Measurement

NCEI: National Centers for Environmental Information

YRB: Yangtze River Basin

AWS: automatic weather station

VNMHA: Vietnam Meteorological and Hydrological Administration

WGAN: Wasserstein generative adversarial network

STPF: short-term precipitation forecast

MMF: multimodal fusion

KMA: Korea Meteorological Administration

ALPF: advanced lightweight precipitation forecasting

SEVIR: Storm Event Imagery Dataset Veillette et al. [2020]

ENCAST: Ensemble NowCASTing

ATWT: à trous wavelet transform

IMERG: Integrated Multi-satellite Retrievals for Global Precipitation Measurement

CMA: China Meteorological Administration

GLDAS: Global Land Data Assimilation System

GEFS: Global Ensemble Forecast System

FMI: Finnish Meteorological Institute

RRDBNet: Residual-in-Residual Dense Block based Network

SCSSA: Sparrow optimization algorithm incorporating positive cosine and Cauchy variants

BILSTM: bi-directional LSTM

WSR-88D: Weather Surveillance Radar-1988 Doppler

NASA: National Aeronautics and Space Administration

JAXA: Japan Aerospace Exploration Agency

pySTEP: An open-source Python library for probabilistic precipitation nowcasting Pulkkinen et al. [2019]

HRES: ECMWF's High Resolution model

Appendix 2: List of Supplement References

Supplement references are listed in Table II.

Appendix 3: List of Evaluation Metrics

Evaluation metrics are listed in Table III.

Dataset	Temporal Range	Spatial Area	Model Type	Evaluation Metrics	ref
PRISM/West-WRF dataset	1985–2019	Western United States	U-Net CNN	RMSE, MAE, BIAS, CSI, PC	Badrinath et al. Badrinath et al. [2023]
Hurricane events from National Hurricane Center, Hurricane rainfall image dataset from the IMERG-E	2002–2019	Gulf of Mexico	CNN	BIAS, MSE, NSE	Kim et al. Kim et al. [2022]
Atmospheric variables from ERA5/Rain gauge data from CMA	1960–2015	Central-Eastern China	MLP-CNN	Accuracy, Recall, AUC, S	Jiang et al. Jiang et al. [2024]
Grid data from ECMWF/Meteorological data from local stations	2013–2019	Longzhong Loess Plateau region, China	CNN-LSTM	Accuracy, Precision, Recall, F_1 , CSI	Li et al. Li [2022b]
Meteorological observation data from China Ground Cumulative Daily Value 1953–2019 Dataset (V3.0)	1953–2019	Kunming, China	PCA-CNN-BiLSTM-Attention	NSE, MAE, RMSE, CC, α , β	Guo et al. Guo et al. [2025]
Precipitation data from ERA5	1979–2019	China	CBAM-CNN	PCC, RMSE	Jin et al. Jin et al. [2022]
Fengyun 4A Satellite Data/Precipitation data from IMERG	2018–2021	Southeast coast of China	Attention-Unet	POD, CSI, FAR, RMSE, CC	Gao et al. Gao et al. [2022b]
Monthly data from CEH-GEAR/Meteorological data from ECMWF SEAS5	1993–2017	Great Britain	CNN	MAR, PRE, PME	Barnes et al. Barnes et al. [2023]
Radar data from FMI	2019–2021	The Baltics and Finland	Lagrangian CNN (L-CNN)	POD, FAR, ETS, FSS, MAE, ME	Ritvanen et al. Ritvanen et al. [2023]
GOES IR images, NCEP Stage IV, PERSIANN-CCS	2016–2017	A central region in the United States	PEISCNN	POD, FAR, CSI, RMSE, ME, OE, UE, HPB, HNB, FB, MB	Yi et al. Yi et al. [2023]
Gauged data from CMA, Interpolated grid data from CN05.1, Satellite data from GPM, Downscaling data from ERA5	1961–2020	Tibetan Plateau, China	CNN, ANN, ETC(statistical)	CC, BIAS, STDRATIO, MAE, RMSE, POD, FAR, CSI, NSE, PBIAS, KGE	Nan et al. Nan et al. [2023]
Cloud image from IoT sensor/Rainfall data acquired from AWS	2020	Seoul, Korea	CNN	MSE	Byun et al. Byun et al. [2023]

Continued on next page

Table 2 – *Continued from previous page*

Dataset	Temporal Range	Spatial Area	Model Type	Evaluation Metrics	ref
Gauge precipitation data/Radar precipitation data from VNMHA/Satellite data from PERSIANN-CCS, GSMP-NRT and IMERG-E	2019–2023	North Central Region, Vietnam	CNN	POD, FAR, BIAS, CSI, MAE, RMSE, CC, mKGE	Bui et al.Bui et al. [2025]
GEFS v2/ERA5	1985–2019	Sacramento River Basin, United States	CNN combined with MLP	F1 Score, AUC	Zhang et al.Zhang et al. [2022]
Data from ERA5 and IMERG	2001–2020	The middle reaches of the Yellow River, China	RRDBNet (CNN based)	RMSE, CC, percentage bias	Fu et al.Fu et al. [2024]
HKO-7/DWD-12/MeteoNet/Brasil	2009–2015/2006–2017/2016–2018/2015–2019	HongKong, China/Germany/France/São Paulo, Brazil	PrecipLSTM	HSS, CSI	Ma et al.Ma et al. [2022]
ERA5, IMERG, and GLDAS	2013–2017	Qinghai Province, China	3D CNN and bidirectional ConvLSTM	MAE, RMSE, CC	You et al.You et al. [2025]
Data from local meteorological stations	1961–2020	Changde, China	CEEMD-PSO-LSTM	RMSE, MAE, MAPE	X. JiangJiang [2023]
Precipitation data provided by the authors	1951–2021	Ankang City, and Yongding District, China	VMD-MSMA-LSTM-ARIMA	RMSE, MAPE, MAE, R^2 , NSE, PICP, MPI	Cui et al.Cui et al. [2023]
Data of various local rainfall stations	2000–2019	Luoyang City, China	EMD-VMD-LSTM	RMSE, δ	Guo et al.Guo et al. [2023]
Data collected by ground weather stations	2018–2019	North China	3D-SA-LSTM	CSI, HSS, FAR, POD	Chen et al.Chen et al. [2022]
Local weather radar data	2020	Guizhou, China	LSTM	CC, MRE, MAE, RMSE	Wang et al.Wang et al. [2023]
Tropical Cyclone Precipitation Dataset (TCPD)	2017–2019	Northwest Pacific	Spatio-temporal Graph-guided Convolutional LSTM	MSE, MAE	Yang et al.Yang et al. [2022]
Monthly precipitation data from NCEI	1973–2021	Luoyang City, China	EEMD-LSTM-ARIMA	RMSE, MAE, MSE, R^2	Zhao et al.Zhao et al. [2022]

Continued on next page

Table 2 – *Continued from previous page*

Dataset	Temporal Range	Spatial Area	Model Type	Evaluation Metrics	ref
Real-world radar echo map dataset provided by the authors	2014–2018	Guangdong province, China	Multiscale WGAN	HSS, CSI, POD, FAR	Luo et al. Luo et al. [2022a]
Radar reflectivity data/Precipitation data from regional AWSs provided by the authors	May to September 2018	Southeastern in 2017 and region of China	STPF-Net	CSI, POD, FAR, BIAS, HSS, BMSE, BMAE	Wang et al. Wang et al. [2024]
Radar echo data from the CIKM AnalytiCup 2017	A total time span of 3 years	Multiple sites	PredRANN	MSE, B-MSE, SSIM, HSS, CSI	Luo et al. Luo et al. [2022b]
RAIN-F dataset from KMA	2017–2019	Korean Peninsula	MMF-RNN	CSI, HSS, PSNR, B-MAE, B-MSE	Liu et al. Liu et al. [2025]
SEVIR dataset	2017–2019	Contiguous US	ALPF (CNN based)	RMSE, SSIM, PSNR, LPIPS	Yang et al. Yang et al. [2024]
WSR-88D radar data/local rain gauge data	2016–2019	Florida Peninsula, United States	RQPENet	RMSE, MAE, CC, NSE, BIAS, POD, FAR, CSI, HSS	Li et al. Li et al. [2023b]
Measured monthly rainfall data from the authors	1996–2020	Xi'an City, China	SCSSA-CNN-BILSTM	R^2 , RMSE, MAE	Zhang et al. Zhang et al. [2024]

Table II: Supplement references for this review.

Metric	Formula	Description
RMSE (Root Mean Square Error)	$\sqrt{\frac{1}{N} \sum_{i=1}^N (P_i - O_i)^2}$	Overall magnitude of prediction errors. Here, P_i = predicted value, O_i = observed value, N = total samples.
MSE (Mean Square Error)	$\frac{1}{N} \sum_{i=1}^N (P_i - O_i)^2$	Average squared error. Here, P_i = predicted value, O_i = observed value, N = total samples.
MAE (Mean Absolute Error)	$\frac{1}{N} \sum_{i=1}^N P_i - O_i $	Average absolute error magnitude. Here, P_i = predicted value, O_i = observed value, N = total samples.
PRE	$\frac{\text{MAE}(p_i, \hat{p}_i)}{\bar{p}_i}$	The proportional regional error for region i . Here, p_i is the benchmark rainfall series, \hat{p}_i is the predicted rainfall series, and \bar{p}_i is the mean benchmark rainfall for region i , respectively.
PME	$\frac{\text{MAE}(p_m, \hat{p}_m)}{\bar{p}_m}$	The proportional monthly error for month m . Here, p_m is the benchmark rainfall series, \hat{p}_m is the predicted rainfall series, and \bar{p}_m is the mean benchmark rainfall for month m , respectively.
ME (Mean Error)	$\frac{1}{N} \sum_{i=1}^N (P_i - O_i)$	Average bias of predictions. Here, P_i = predicted value, O_i = observed value, N = total samples.
B-MAE	$\frac{1}{C} \sum_{c=1}^C \frac{1}{n_c} \sum_{i=1}^{n_c} P_i^{(c)} - O_i^{(c)} $	Balanced Mean Absolute Error, here C is the number of classes; n_c is the number of samples in class c ; $P_i^{(c)}$ and $O_i^{(c)}$ denote the predicted and observed values, respectively, for the i -th sample in class c .
B-MSE	$\frac{1}{C} \sum_{c=1}^C \frac{1}{n_c} \sum_{i=1}^{n_c} (P_i^{(c)} - O_i^{(c)})^2$	Balanced Mean Squared Error, here C is the number of classes; n_c is the number of samples in class c ; $P_i^{(c)}$ and $O_i^{(c)}$ denote the predicted and observed values, respectively, for the i -th sample in class c .
FSS (Fraction Skill Score)	$1 - \frac{\frac{1}{N} \sum_{i=1}^N (P_i - O_i)^2}{\frac{1}{N} \sum_{i=1}^N (P_i^2 + O_i^2)}$	The Fraction Skill Score evaluates the spatial agreement between predicted and observed precipitation fields after neighborhood smoothing. Here, P_i = predicted value, O_i = observed value, N = total samples.
MAPE (Mean Absolute Percentage Error)	$\frac{100\%}{N} \sum_{i=1}^N \left \frac{P_i - O_i}{O_i} \right $	Average absolute percentage difference between predicted and actual values. Here, P_i = predicted value, O_i = observed value, N = total samples.

Continued on next page

Table 3 – *Continued from previous page*

Metric	Formula	Description
R^2 (Coefficient of Determination)	$1 - \frac{\sum_{i=1}^N (P_i - O_i)^2}{\sum_{i=1}^N (O_i - \bar{O})^2}$	Proportion of variance in observed data explained by the predictions. Here, P_i = predicted value, O_i = observed value, N = total samples.
BIAS	$\frac{\sum_{i=1}^N P_i}{\sum_{i=1}^N O_i}$	Overestimation/underestimation. Here, P_i = predicted value, O_i = observed value, N = total samples.
Relative Bias	$\frac{\sum_{i=1}^N P_i}{\sum_{i=1}^N O_i} - 1$	Relative overestimation/underestimation. Here, P_i = predicted value, O_i = observed value, N = total samples.
CSI (Critical Success Index)	$\frac{H}{H + M + F}$	Fraction of observed events correctly predicted. Here, H = correctly predicted (hits), M = misses, F = false alarms.
PC (Probability of Correct)	$\frac{H + C}{N}$	Overall accuracy (hits + correct negatives). Here, H = correctly predicted (hits), C = correct negatives, N = total samples.
CC (Correlation Coefficient)	$\frac{\sum_{i=1}^N (P_i - \bar{P})(O_i - \bar{O})}{\sqrt{\sum_{i=1}^N (P_i - \bar{P})^2 \sum_{i=1}^N (O_i - \bar{O})^2}}$	Linear association between prediction and observation. Here, P_i = predicted value, O_i = observed value, \bar{P} = mean of all predicted values, \bar{O} = mean of all observed values, N = total samples.
POD (Probability of Detection)	$\frac{H}{H + M}$	Fraction of observed events that were predicted. Here, H = correctly predicted (hits), M = misses.
POFD (Probability of False Detection)	$\frac{F}{F + C}$	Fraction of non-events incorrectly predicted as events. Here, F = false alarms, C = correct negatives.
FAR (False Alarm Ratio)	$\frac{F}{H + F}$	Fraction of predicted events that did not occur. Here, F = false alarms, H = correctly predicted (hits).
SR (SuccessRatio)	$\frac{H}{H + F}$	Fraction of the forecasted precipitation events that were correctly observed. Here, F = false alarms, H = correctly predicted (hits).
HSS (Heidke Skill Score)	$\frac{2(HC - MF)}{(H + M)(M + C) + (H + F)(F + C)}$	Skill score adjusted for random chance. Here, H = hits, M = misses, F = false alarms, C = correct negatives.

Continued on next page

Table 3 – *Continued from previous page*

Metric	Formula	Description
NSE (Nash-Sutcliffe Efficiency)	$1 - \frac{\sum_{i=1}^N (O_i - P_i)^2}{\sum_{i=1}^N (O_i - \bar{O})^2}$	Predictive skill vs. mean observation. Here, P_i = predicted value, O_i = observed value, N = number of samples.
Accuracy	$\frac{TN + TP}{n} \times 100\%$	Percentage of all samples correctly classified. Here, TN = true negatives, TP = true positives, n = total number of predictions.
S (Positive Rank Sum)	$\sum_{i \in \text{positives}} \text{rank}_i$	Sum of the ranks assigned to positive instances when all samples are ranked by score.
AUC (Area Under ROC Curve)	$\frac{S - \frac{P(P+1)}{2}}{N \times P}$	Probability that a randomly chosen positive ranks higher than a randomly chosen negative. Here, S is Positive Rank Sum, and $P(N)$ represent the number of positive (negative) events.
Recall (Sensitivity)	$\frac{TP}{TP + FN} \times 100\%$	Fraction of actual positives that are correctly identified. Here, TP = true positives, FN = false negatives.
Precision	$\frac{TP}{TP + FP} \times 100\%$	Fraction of predicted positives that are actual positives. Here, TP = true positives, FP = false positives.
F_1	$2 \times \frac{\text{Precision} \times \text{Recall}}{\text{Precision} + \text{Recall}}$	Harmonic mean of Precision and Recall (denoted above), balancing both metrics.
PBIAS (Percent Bias/Water Volume Error)	$100 \times \frac{\sum_{i=1}^N (P_i - O_i)}{\sum_{i=1}^N O_i}$	Percentage bias of predicted volume relative to the observed; positive values indicate overestimation, while negative values indicate underestimation. Here, P_i = predicted value, O_i = observed value, N = number of samples.
α	$\frac{\sigma_p}{\sigma_o}$	σ_p and σ_o are the standard values of predicted and simulated precipitation, respectively
β	$\frac{y_{p,i} - y_{o,i}}{y_{o,i}}$	$y_{p,i}$ and $y_{o,i}$ are the simulated value of precipitation and observed value of precipitation at time i , respectively

Continued on next page

Table 3 – *Continued from previous page*

Metric	Formula	Description
KGE (Kling-Gupta Efficiency)	$\sqrt{1 - \frac{(CC - 1)^2 + \left(\frac{\sigma_P}{\sigma_O} - 1\right)^2 + \left(\frac{\mu_P}{\mu_O} - 1\right)^2}{3}}$	Composite metric combining correlation CC , variability ratio, and bias ratio to assess agreement between predictions and observations. Here, σ_P and σ_O are standard deviations for predictions and observations, respectively. μ_P and μ_O are means of predictions and observations, respectively. CC is the Correlation Coefficient denoted above.
mKGE (modified Kling-Gupta Efficiency)	$\sqrt{1 - \frac{(CC - 1)^2 + \left(\frac{\sigma_P/\mu_P}{\sigma_O/\mu_O} - 1\right)^2 + \left(\frac{\mu_P}{\mu_O} - 1\right)^2}{3}}$	A modified version of KGE , which ensures that the bias and variability ratios are not cross-correlated. Here, σ_P and σ_O are standard deviations for predictions and observations, respectively. μ_P and μ_O are means of predictions and observations, respectively. CC is the Correlation Coefficient denoted above.
OE (Overestimation)	$HPB + FB$	Total positive bias from HPB and FB. HPB and FB are components from 4CEDZhang et al. [2021b]
UE (Underestimation)	$HNB + MB$	Total negative bias from HNB and MB. HNB and MB are components from 4CEDZhang et al. [2021b]
ETS/GSS	$\frac{TP - R}{TP + FP + FN - R}$	The Equitable Threat Score (ETS)/Gilbert skill score (GSS) measures forecast skill relative to random chance. Here, TP = true positives, FP = false positives, FN = false negatives, $R = \frac{(TP+FP)(TP+FN)}{\text{Total}}$
PICP (Prediction Interval Coverage Probability)	$\frac{1}{n} \sum_{i=1}^n c_i$	Measures the proportion of ground truth values that fall within their corresponding prediction intervals. Here, $c_i = 1$ is the judgement coefficient if P_i lies in the prediction interval, otherwise $c_i = 0$.
MPI (Mean Prediction Interval)	$2 \cdot t_{n-p}^{\alpha/2} \cdot \left(\frac{1}{n} \sum_{i=1}^n s_i \right)$	Measures the average width of the prediction intervals across all samples. The coefficient $t_{n-p}^{\alpha/2}$ is the t -distribution with $n - p$ degrees of freedom for $(1 - \alpha)\%$.

Continued on next page

Table 3 – *Continued from previous page*

Metric	Formula	Description
δ (Actual Relative Error)	$\frac{\Delta}{L} \times 100\%$	Refers to the value obtained by multiplying the absolute error Δ caused by the measurement by the ratio of the measured (conventional) true value L , and then multiplying by 100%, expressed in percentage.
PSNR (Peak Signal-to-Noise Ratio)	$10 \cdot \log_{10} \left(\frac{MAX_I^2}{MSE} \right)$	where MAX_I is the maximum possible pixel value of the image (for example, $MAX_I = 255$ for 8-bit grayscale images). Higher PSNR values indicate greater similarity (less distortion).
SSIM (Structural Similarity Index)	$\frac{(2\mu_x\mu_y + C_1)(2\sigma_{xy} + C_2)}{(\mu_x^2 + \mu_y^2 + C_1)(\sigma_x^2 + \sigma_y^2 + C_2)}$	Where μ_x, μ_y are the mean intensities of x and y , σ_x^2, σ_y^2 are their variances, σ_{xy} is the covariance between x and y , C_1, C_2 are small constants to stabilize the division. SSIM values range from -1 to 1 . A value of 1 indicates perfect similarity, while values close to 0 or negative indicate poor structural similarity.
LPIPS (Structural Similarity Index)	$\sum_l \frac{1}{H_l W_l} \sum_{h,w} \ (\hat{y}_l(x)_{hw} - \hat{y}_l(y)_{hw})\ _2^2$	Where $\hat{y}_l(x)$ and $\hat{y}_l(y)$ are unit-normalized feature maps from layer l of the network, H_l, W_l are spatial dimensions of the feature map at layer l , w_l are learned weights that calibrate the contribution of each channel. LPIPS has been shown to correlate strongly with human perceptual studies. Lower LPIPS score indicates higher perceptual similarity.

Table III: Evaluation metrics for neural network precipitation models.

References

Ryan L. Li, Joshua H. P. Studholme, Alexey V. Fedorov, and Trude Storelvmo. Precipitation efficiency constraint on climate change. *Nature Climate Change*, 12:642–648, 2022a. ISSN 1758-6798. doi:10.1038/s41558-022-01400-x.

W. Schröder. History of geophysics. *Acta Geodaetica et Geophysica Hungarica*, 45(2):253–261, 2010. doi:10.1556/ageod.45.2010.2.9. URL <https://akjournals.com/view/journals/074/45/2/article-p253.xml>.

Thomas M. Mitchell. *Machine Learning*. McGraw-Hill, Inc., USA, 1 edition, 1997. ISBN 0070428077.

M.H. Glantz. *Currents of Change: Impacts of El Niño and La Niña on Climate and Society*. Cambridge University Press, 2001. ISBN 9780521786720.

Kevin E. Trenberth and David P. Stepaniak. The flow of energy through the earth’s climate system. *Quarterly Journal of the Royal Meteorological Society*, 130(603):2677–2701, 2004. doi:<https://doi.org/10.1256/qj.04.83>.

Kristine C. Harper. The history of synoptic meteorology in the age of numerical weather forecasting, 04 2024.

J. Shukla and J. L. Kinter. *Predictability of seasonal climate variations: a pedagogical review*, pages 306–341. Cambridge University Press, 2006.

Allan H. Murphy. Skill scores based on the mean square error and their relationships to the correlation coefficient. *Monthly Weather Review*, 116(12):2417–2424, 1988. doi:10.1175/1520-0493(1988)116<2417:SSBOTM>2.0.CO;2.

Eugenia Kalnay. *Atmospheric Modeling, Data Assimilation and Predictability*. Cambridge University Press, 2002a.

F. Zhang, Chris Snyder, and Richard Rotunno. Effects of moist convection on mesoscale predictability. *Journal of the Atmospheric Sciences*, 60(9):1173–1185, 2003. doi:10.1175/1520-0469(2003)060<1173:EOMCOM>2.0.CO;2. URL https://journals.ametsoc.org/view/journals/atsc/60/9/1520-0469_2003_060_1173_eomcom_2.0.co_2.xml.

P. L. Houtekamer and Fuqing Zhang. Review of the ensemble kalman filter for atmospheric data assimilation. *Monthly Weather Review*, 144(12):4489–4532, 2016. doi:10.1175/MWR-D-15-0440.1. URL <https://journals.ametsoc.org/view/journals/mwre/144/12/mwr-d-15-0440.1.xml>.

T N Palmer. Predicting uncertainty in forecasts of weather and climate. *Reports on Progress in Physics*, 63(2):71, feb 2000. doi:10.1088/0034-4885/63/2/201. URL <https://dx.doi.org/10.1088/0034-4885/63/2/201>.

Enzo Pinheiro and Taha B. M. J. Ouarda. An interpretable machine learning model for seasonal precipitation forecasting. *Communications Earth & Environment*, 6, 2025. ISSN 2662-4435. doi:10.1038/s43247-025-02207-2.

J.B. Campbell and R.H. Wynne. *Introduction to Remote Sensing*. Guilford Publications, 2011. ISBN 9781609181765. URL <https://books.google.ca/books?id=zgQDZEya6foC>.

T. Lillesand, R. Kiefer, and J. Chipman. *Remote Sensing and Image Interpretation*. 7th ed. Wiley, 2015.

James R. Irons, John L. Dwyer, and Julia A. Barsi. The next landsat satellite: The landsat data continuity mission. *Remote Sensing of Environment*, 122:11–21, 2012. ISSN 0034-4257. doi:<https://doi.org/10.1016/j.rse.2011.08.026>. URL <https://www.sciencedirect.com/science/article/pii/S0034425712000363>. Landsat Legacy Special Issue.

John A. Richards. *Remote Sensing Digital Image Analysis: An Introduction*. Springer Berlin, Heidelberg, 2014.

Xiaolin Zhu, Fangyi Cai, Jiaqi Tian, and Trecia Kay-Ann Williams. Spatiotemporal fusion of multisource remote sensing data: Literature survey, taxonomy, principles, applications, and future directions. *Remote Sensing*, 10(4), 2018. ISSN 2072-4292. doi:10.3390/rs10040527. URL <https://www.mdpi.com/2072-4292/10/4/527>.

Rolf H. Reichle, Dennis B. McLaughlin, and Dara Entekhabi. Hydrologic data assimilation with the ensemble kalman filter. *Monthly Weather Review*, 130(1):103–114, 2002. doi:10.1175/1520-0493(2002)130<0103:HDAWTE>2.0.CO;2. URL https://journals.ametsoc.org/view/journals/mwre/130/1/1520-0493_2002_130_0103_hdawte_2.0.co_2.xml.

Lei Ma, Yu Liu, Xueliang Zhang, Yuanxin Ye, Gaofei Yin, and Brian Alan Johnson. Deep learning in remote sensing applications: A meta-analysis and review. *ISPRS Journal of Photogrammetry and Remote Sensing*, 152:166–177, 2019. ISSN 0924-2716. doi:<https://doi.org/10.1016/j.isprsjprs.2019.04.015>. URL <https://www.sciencedirect.com/science/article/pii/S0924271619301108>.

Kaifeng Bi, Lingxi Xie, Hengheng Zhang, Xin Chen, Xiaotao Gu, and Qi Tian. Accurate medium-range global weather forecasting with 3d neural networks. *Nature*, 619:533–538, 2023a. ISSN 1476-4687. doi:10.1038/s41586-023-06185-3.

Casper Kaae Sønderby, Lasse Espeholt, Jonathan Heek, Mostafa Dehghani, Avital Oliver, Tim Salimans, Shreya Agrawal, Jason Hickey, and Nal Kalchbrenner. Metnet: A neural weather model for precipitation forecasting, 2020. URL <https://arxiv.org/abs/2003.12140>.

Sahil Gujral, Darshan Rao, Anuj Khanvilkar, Umit Shah, and Tabassum Maktum. Tci-net: A deep learning approach for tropical cyclone intensity prediction. In *2023 International Conference on Network, Multimedia and Information Technology (NMITCON)*, pages 1–7, 2023. doi:10.1109/NMITCON58196.2023.10276163.

S.L. Gan, J.Y. Fu, G.F. Zhao, P.W. Chan, and Y.C. He. Short-term prediction of tropical cyclone track and intensity via four mainstream deep learning techniques. *Journal of Wind Engineering and Industrial Aerodynamics*, 244:105633, 2024. ISSN 0167-6105. doi:<https://doi.org/10.1016/j.jweia.2023.105633>. URL <https://www.sciencedirect.com/science/article/pii/S0167610523003355>.

Dmitrii Shadrin, Svetlana Illarionova, Fedor Gubanov, Ksenia Evteeva, Maksim Mironenko, Ivan Levchunets, Roman Belousov, and Evgeny Burnaev. Wildfire spreading prediction using multimodal data and deep neural network approach. *Scientific Reports*, 14:2606, 2024. ISSN 2045-2322. doi:10.1038/s41598-024-52821-x.

Hongtao Xiao, Yingfang Zhu, Yurong Sun, Gui Zhang, and Zhiwei Gong. Wildfire spread prediction using attention mechanisms in u2-net. *Forests*, 15(10), 2024. ISSN 1999-4907. doi:10.3390/f15101711. URL <https://www.mdpi.com/1999-4907/15/10/1711>.

Nasreddine Belabid, Feng Zhao, Luca Brocca, Yanbo Huang, and Yumin Tan. Near-real-time flood forecasting based on satellite precipitation products. *Remote Sensing*, 11(3), 2019. ISSN 2072-4292. doi:10.3390/rs11030252. URL <https://www.mdpi.com/2072-4292/11/3/252>.

Minjie Zhang, Xiang Fu, Shuangjun Liu, and Can Zhang. Integrating remote sensing and machine learning for actionable flood risk assessment: Multi-scenario projection in the ili river basin in china under climate change. *Remote Sensing*, 17(7), 2025. ISSN 2072-4292. doi:10.3390/rs17071189. URL <https://www.mdpi.com/2072-4292/17/7/1189>.

Francesca Rochberg. *The Heavenly Writing: Divination, Horoscopy, and Astronomy in Mesopotamian Culture*. Cambridge University Press, 2004.

Malcolm Wilson. *Structure and Method in Aristotle's Meteorologica: A More Disorderly Nature*. Cambridge University Press, 2013.

Joseph Needham and Wang Ling. *Science and Civilisation in China: Volume 3, Mathematics and the Sciences of the Heavens and the Earth*. Cambridge University Press, 1959.

George Saliba. *Islamic Science and the Making of the European Renaissance*. The MIT Press, 03 2007. ISBN 9780262282888. doi:10.7551/mitpress/3981.001.0001. URL <https://doi.org/10.7551/mitpress/3981.001.0001>.

Nicholas Campion. *History of western astrology. The medieval and modern worlds. Volume II*. Continuum, 2009. ISBN 1-282-87118-8.

Robert Marc Friedman. *Appropriating the Weather: Vilhelm Bjerknes and the Construction of a Modern Meteorology*. Cornell University Press, 1989.

Peter Lynch. The origins of computer weather prediction and climate modeling. *Journal of Computational Physics*, 227(7):3431–3444, 2008a. ISSN 0021-9991. doi:<https://doi.org/10.1016/j.jcp.2007.02.034>. URL <https://www.sciencedirect.com/science/article/pii/S0021999107000952>. Predicting weather, climate and extreme events.

Martin H. Weik. The eniac story. *Ordnance*, 45(244):571–575, 1961. ISSN 00304557. URL <http://www.jstor.org/stable/45363261>.

Peter Lynch. The eniac forecasts: A re-creation. *Bulletin of the American Meteorological Society*, 89(1):45–56, 2008b. doi:10.1175/BAMS-89-1-45. URL <https://journals.ametsoc.org/view/journals/bams/89/1/bams-89-1-45.xml>.

J. G. Charney, R. Fjörtoft, and J. Von Neumann and. Numerical integration of the barotropic vorticity equation. *Tellus*, 2(4):237–254, 1950. doi:10.3402/tellusa.v2i4.8607.

Brian Golding, Kenneth Mylne, and Peter Clark. The history and future of numerical weather prediction in the Met Office. *Weather*, 59(11):299–306, November 2004. doi:10.1256/wea.113.04.

Kristine Harper, Louis W. Uccellini, Eugenia Kalnay, Kenneth Carey, and Lauren Morone. 50th anniversary of operational numerical weather prediction. *Bulletin of the American Meteorological Society*, 88(5):639–650, 2007. doi:10.1175/BAMS-88-5-639. URL <https://journals.ametsoc.org/view/journals/bams/88/5/bams-88-5-639.xml>.

F. Nebeker. *Calculating the Weather: Meteorology in the 20th Century*. International Geophysics. Academic Press, 1995. ISBN 9780080528410.

Anders Persson. Early operational numerical weather prediction outside the usa: an historical introduction: Part ii: Twenty countries around the world. *Meteorological Applications*, 12(3):269–289, 2005. doi:<https://doi.org/10.1017/S1350482705001751>. URL <https://rmets.onlinelibrary.wiley.com/doi/abs/10.1017/S1350482705001751>.

Eugenia Kalnay. *Atmospheric Modeling, Data Assimilation and Predictability*. Cambridge University Press, 2002b.

T N Krishnamurti, H S Bedi, and V M Hardiker. *An Introduction to Global Spectral Modeling*. Oxford University Press, 05 1998. ISBN 9780195094732. doi:10.1093/oso/9780195094732.001.0001. URL <https://doi.org/10.1093/oso/9780195094732.001.0001>.

Tim Palmer. The ecmwf ensemble prediction system: Looking back (more than) 25 years and projecting forward 25 years. *Quarterly Journal of the Royal Meteorological Society*, 145(S1):12–24, 2019. doi:<https://doi.org/10.1002/qj.3383>. URL <https://rmets.onlinelibrary.wiley.com/doi/abs/10.1002/qj.3383>.

Harry R. Glahn and Dale A. Lowry. The use of model output statistics (mos) in objective weather forecasting. *Journal of Applied Meteorology and Climatology*, 11(8):1203–1211, 1972. doi:10.1175/1520-0450(1972)011<1203: TUOMOS>2.0.CO;2. URL https://journals.ametsoc.org/view/journals/apme/11/8/1520-0450_1972_011_1203_tuomos_2_0_co_2.xml.

Jan John and Josef Štekł. Nonlinear adaptive regression predictors based on singular decomposition. *Studia Geophysica et Geodaetica*, 34:369–378, 1990. ISSN 1573-1626. doi:10.1007/BF02316956.

Yongqiang Liu. Prediction of monthly-seasonal precipitation using coupled svd patterns between soil moisture and subsequent precipitation. *Geophysical Research Letters*, 30(15), 2003. doi:<https://doi.org/10.1029/2003GL017709>. URL <https://agupubs.onlinelibrary.wiley.com/doi/abs/10.1029/2003GL017709>.

Cornel Soci, Hans Hersbach, Adrian Simmons, Paul Poli, Bill Bell, Paul Berrisford, András Horányi, Joaquín Muñoz Sabater, Julien Nicolas, Raluca Radu, Dinand Schepers, Sébastien Villaume, Leopold Haimberger, Jack Woollen, Carlo Buontempo, and Jean-Noël Thépaut. The era5 global reanalysis from 1940 to 2022. *Quarterly Journal of the Royal Meteorological Society*, 150(764):4014–4048, 2024. doi:<https://doi.org/10.1002/qj.4803>. URL <https://rmets.onlinelibrary.wiley.com/doi/abs/10.1002/qj.4803>.

S. J. Johnson, T. N. Stockdale, L. Ferranti, M. A. Balmaseda, F. Molteni, L. Magnusson, S. Tietsche, D. DeClerk, A. Weisheimer, G. Balsamo, S. P. E. Keeley, K. Mogensen, H. Zuo, and B. M. Monge-Sanz. Seas5: the new ecmwf seasonal forecast system. *Geoscientific Model Development*, 12(3):1087–1117, 2019. doi:10.5194/gmd-12-1087-2019. URL <https://gmd.copernicus.org/articles/12/1087/2019/>.

Christopher Daly, Matthew K. Doggett, Joseph I. Smith, Keith V. Olson, Michael D. Halbleib, Zlatko Dimcovic, Dylan Keon, Rebecca A. Loiselle, Ben Steinberg, Adam D. Ryan, Cherri M. Pancake, and Eileen M. Kaspar. Challenges in observation-based mapping of daily precipitation across the conterminous united states. *Journal of Atmospheric and Oceanic Technology*, 38(11):1979–1992, 2021. doi:10.1175/JTECH-D-21-0054.1. URL <https://journals.ametsoc.org/view/journals/atot/38/11/JTECH-D-21-0054.1.xml>.

George J. Huffman, David T. Bolvin, Dan Braithwaite, Kuo-Lin Hsu, Robert J. Joyce, Christopher Kidd, Eric J. Nelkin, Soroosh Sorooshian, Erich F. Stocker, Jackson Tan, David B. Wolff, and Pingping Xie. *Integrated Multi-satellite Retrievals for the Global Precipitation Measurement (GPM) Mission (IMERG)*, pages 343–353. Springer International Publishing, Cham, 2020. ISBN 978-3-030-24568-9. doi:10.1007/978-3-030-24568-9_19. URL https://doi.org/10.1007/978-3-030-24568-9_19.

Mark S. Veillette, Siddharth Samsi, and Christopher J. Mattioli. Sevir: a storm event imagery dataset for deep learning applications in radar and satellite meteorology. In *Proceedings of the 34th International Conference on Neural Information Processing Systems*, NIPS '20, Red Hook, NY, USA, 2020. Curran Associates Inc. ISBN 9781713829546.

Tao Chen and M. Takagi. Rainfall prediction of geostationary meteorological satellite images using artificial neural network. In *Proceedings of IGARSS '93 - IEEE International Geoscience and Remote Sensing Symposium*, pages 1247–1249 vol.3, 1993. doi:10.1109/IGARSS.1993.322107.

Kou lin Hsu, Xiaogang Gao, Soroosh Sorooshian, and Hoshin V. Gupta. Precipitation estimation from remotely sensed information using artificial neural networks. *Journal of Applied Meteorology*, 36(9):1176–1190, 1997. doi:10.1175/1520-0450(1997)036<1176:PEFRSI>2.0.CO;2. URL https://journals.ametsoc.org/view/journals/apme/36/9/1520-0450_1997_036_1176_pefrsi_2_0.co_2.xml.

Bernard N. Meisner and Phillip A. Arkin. Spatial and annual variations in the diurnal cycle of large-scale tropical convective cloudiness and precipitation. *Monthly Weather Review*, 115(9):2009–2032, 1987. doi:10.1175/1520-0493(1987)115<2009:SAAVIT>2.0.CO;2.

Mary N. Ahuna, Thomas J. Afullo, and Akintunde A. Alonge. Rainfall rate prediction based on artificial neural networks for rain fade mitigation over earth-satellite link. In *2017 IEEE AFRICON*, pages 579–584, 2017. doi:10.1109/AFRCON.2017.8095546.

Yuzhong Peng, Daoqing Gong, Chuyan Deng, Hongya Li, Hongguo Cai, and Hao Zhang. An automatic hyperparameter optimization dnn model for precipitation prediction. *Applied Intelligence*, 52:2703–2719, 2022a. ISSN 1573-7497. doi:10.1007/s10489-021-02507-y.

D. Vasudeva Rayudu and J Femila Roseline. Accurate weather forecasting for rainfall prediction using artificial neural network compared with deep learning neural network. In *2023 International Conference on Artificial Intelligence and Knowledge Discovery in Concurrent Engineering (ICECONF)*, pages 1–6, 2023. doi:10.1109/ICECONF57129.2023.10084252.

T. Cover and P. Hart. Nearest neighbor pattern classification. *IEEE Transactions on Information Theory*, 13(1):21–27, 1967. doi:10.1109/TIT.1967.1053964.

C.I. Christodoulou, S.C. Michaelides, M. Gabella, and C.S. Pattichis. Prediction of rainfall rate based on weather radar measurements. In *2004 IEEE International Joint Conference on Neural Networks (IEEE Cat. No.04CH37541)*, volume 2, pages 1393–1396 vol.2, 2004. doi:10.1109/IJCNN.2004.1380153.

Bagus Setya, Rizqy Agung Nurhidayatullah, Maria Beliti Hewen, and Kusrini Kusrini. Comparative analysis of rainfall value prediction in semarang using linear and k-nearest neighbor algorithms. In *2023 5th International Conference on Cybernetics and Intelligent System (ICORIS)*, pages 1–5, 2023. doi:10.1109/ICORIS60118.2023.10352274.

Y. Lecun, L. Bottou, Y. Bengio, and P. Haffner. Gradient-based learning applied to document recognition. *Proceedings of the IEEE*, 86(11):2278–2324, 1998. doi:10.1109/5.726791.

G. Ayzel, T. Scheffer, and M. Heistermann. Rainnet v1.0: a convolutional neural network for radar-based precipitation nowcasting. *Geoscientific Model Development*, 13(6):2631–2644, 2020. doi:10.5194/gmd-13-2631-2020. URL <https://gmd.copernicus.org/articles/13/2631/2020/>.

Mojtaba Sadeghi, Ata Akbari Asanjan, Mohammad Faridzad, Phu Nguyen, Kuolin Hsu, Soroosh Sorooshian, and Dan Braithwaite. Persiann-cnn: Precipitation estimation from remotely sensed information using artificial neural networks–convolutional neural networks. *Journal of Hydrometeorology*, 20(12):2273–2289, 2019. doi:10.1175/JHM-D-19-0110.1. URL https://journals.ametsoc.org/view/journals/hdr/20/12/jhm-d-19-0110_1.xml.

Baoxiang Pan, Kuolin Hsu, Amir AghaKouchak, and Soroosh Sorooshian. Improving precipitation estimation using convolutional neural network. *Water Resources Research*, 55(3):2301–2321, 2019. doi:<https://doi.org/10.1029/2018WR024090>.

Cunguang Wang, Jing Xu, Guoqiang Tang, Yi Yang, and Yang Hong. Infrared precipitation estimation using convolutional neural network. *IEEE Transactions on Geoscience and Remote Sensing*, 58(12):8612–8625, 2020. doi:10.1109/TGRS.2020.2989183.

Cunguang Wang, Guoqiang Tang, Wentao Xiong, Ziqiang Ma, and Siyu Zhu. Infrared precipitation estimation using convolutional neural network for fengyun satellites. *Journal of Hydrology*, 603:127113, 2021a. ISSN 0022-1694. doi:<https://doi.org/10.1016/j.jhydrol.2021.127113>. URL <https://www.sciencedirect.com/science/article/pii/S002216942101163X>.

Mei Xue, Renlong Hang, Qingshan Liu, Xiao-Tong Yuan, and Xinyu Lu. Cnn-based near-real-time precipitation estimation from fengyun-2 satellite over xinjiang, china. *Atmospheric Research*, 250:105337, 2021. ISSN 0169-8095. doi:<https://doi.org/10.1016/j.atmosres.2020.105337>. URL <https://www.sciencedirect.com/science/article/pii/S0169809520312746>.

Dan Niu, Li Diao, Liuja Xu, Zengliang Zang, Xisong Chen, and ShaSha Liang. Precipitation forecast based on multi-channel convlstm and 3d-cnn. In *2020 International Conference on Unmanned Aircraft Systems (ICUAS)*, pages 367–371, 2020. doi:10.1109/ICUAS48674.2020.9213930.

Yung-Yun Cheng, Chia-Tung Chang, Buo-Fu Chen, Hung-Chi Kuo, and Cheng-Shang Lee. Extracting 3d radar features to improve quantitative precipitation estimation in complex terrain based on deep learning neural networks. *Weather and Forecasting*, 38(2):273–289, 2023. doi:10.1175/WAF-D-22-0034.1. URL <https://journals.ametsoc.org/view/journals/wefo/38/2/WAF-D-22-0034.1.xml>.

V. N. Vapnik and A. Ya. Chervonenkis. On the uniform convergence of relative frequencies of events to their probabilities. *Theory of Probability & Its Applications*, 16(2):264–280, 1971. doi:10.1137/1116025.

Corinna Cortes and Vladimir Vapnik. Support-vector networks. *Machine Learning*, 20:273–297, 1995. ISSN 1573-0565. doi:10.1007/BF00994018.

Wei-Chiang Hong. Rainfall forecasting by technological machine learning models. *Applied Mathematics and Computation*, 200(1):41–57, 2008. ISSN 0096-3003. doi:<https://doi.org/10.1016/j.amc.2007.10.046>. URL <https://www.sciencedirect.com/science/article/pii/S0096300307010843>.

Kesheng Lu and Lingzhi Wang. A novel nonlinear combination model based on support vector machine for rainfall prediction. In *2011 Fourth International Joint Conference on Computational Sciences and Optimization*, pages 1343–1346, 2011. doi:10.1109/CSO.2011.50.

Gaohong Yin, Takao Yoshikane, Kosuke Yamamoto, Takuji Kubota, and Kei Yoshimura. A support vector machine-based method for improving real-time hourly precipitation forecast in japan. *Journal of Hydrology*, 612:128125, 2022. ISSN 0022-1694. doi:<https://doi.org/10.1016/j.jhydrol.2022.128125>. URL <https://www.sciencedirect.com/science/article/pii/S0022169422007004>.

Gaohong Yin, Takao Yoshikane, Ryo Kaneko, and Kei Yoshimura. Improving global subseasonal to seasonal precipitation forecasts using a support vector machine-based method. *Journal of Geophysical Research: Atmospheres*, 128(17):e2023JD038929, 2023. doi:<https://doi.org/10.1029/2023JD038929>. URL <https://agupubs.onlinelibrary.wiley.com/doi/abs/10.1029/2023JD038929>.

Reza Rezaiy and Ani Shabri. Improving drought prediction accuracy: A hybrid eemd and support vector machine approach with standardized precipitation index. *Water Resources Management*, 38:5255–5277, 2024. ISSN 1573-1650. doi:10.1007/s11269-024-03912-x.

Reza Rezaiy and Ani Shabri. Integrating wavelet transform and support vector machine for improved drought forecasting based on standardized precipitation index. *Journal of Hydroinformatics*, 27(2):320–337, 02 2025. ISSN 1464-7141. doi:10.2166/hydro.2025.292. URL <https://doi.org/10.2166/hydro.2025.292>.

Wei Fang, Yupeng Chen, and Qiongying Xue. Survey on research of rnn-based spatio-temporal sequence prediction algorithms. *Journal on Big Data*, 3(3):97–110, 2021.

Jeffrey L. Elman. Finding structure in time. *Cognitive Science*, 14(2):179–211, 1990. ISSN 0364-0213. doi:[https://doi.org/10.1016/0364-0213\(90\)90002-E](https://doi.org/10.1016/0364-0213(90)90002-E). URL <https://www.sciencedirect.com/science/article/pii/036402139090002E>.

Ian Goodfellow, Yoshua Bengio, and Aaron Courville. *Deep Learning*. MIT Press, 2016.

Zhifeng Ma, Hao Zhang, and Jie Liu. Mm-rnn: A multimodal rnn for precipitation nowcasting. *IEEE Transactions on Geoscience and Remote Sensing*, 61:1–14, 2023. doi:10.1109/TGRS.2023.3264545.

Sepp Hochreiter and Jürgen Schmidhuber. Long short-term memory. *Neural Computation*, 9(8):1735–1780, 1997. doi:10.1162/neco.1997.9.8.1735.

F.A. Gers, J. Schmidhuber, and F. Cummins. Learning to forget: continual prediction with lstm. In *1999 Ninth International Conference on Artificial Neural Networks ICANN 99. (Conf. Publ. No. 470)*, volume 2, pages 850–855 vol.2, 1999. doi:10.1049/cp:19991218.

Xingjian SHI, Zhourong Chen, Hao Wang, Dit-Yan Yeung, Wai-kin Wong, and Wang-chun WOO. Convolutional lstm network: A machine learning approach for precipitation nowcasting. In C. Cortes, N. Lawrence, D. Lee, M. Sugiyama, and R. Garnett, editors, *Advances in Neural Information Processing Systems*, volume 28. Curran Associates, Inc., 2015.

Xingjian Shi, Zhihan Gao, Leonard Lausen, Hao Wang, Dit-Yan Yeung, Wai-kin Wong, and Wang-chun Woo. Deep learning for precipitation nowcasting: A benchmark and a new model. *Advances in neural information processing systems*, 30, 2017.

Yunbo Wang, Mingsheng Long, Jianmin Wang, Zhifeng Gao, and Philip S Yu. Predrnn: Recurrent neural networks for predictive learning using spatiotemporal lstms. In I. Guyon, U. Von Luxburg, S. Bengio, H. Wallach, R. Fergus, S. Vishwanathan, and R. Garnett, editors, *Advances in Neural Information Processing Systems*, volume 30. Curran Associates, Inc., 2017. URL https://proceedings.neurips.cc/paper_files/paper/2017/file/e5f6ad6ce374177eef023bf5d0c018b6-Paper.pdf.

Yunbo Wang, Zhifeng Gao, Mingsheng Long, Jianmin Wang, and Philip S Yu. Predrnn++: Towards a resolution of the deep-in-time dilemma in spatiotemporal predictive learning. In *International conference on machine learning*, pages 5123–5132. PMLR, 2018.

Suzanna Maria Bonnet, Alexandre Evsukoff, and Carlos Augusto Morales Rodriguez. Precipitation nowcasting with weather radar images and deep learning in são paulo, brasil. *Atmosphere*, 11(11), 2020. ISSN 2073-4433. doi:10.3390/atmos11111157. URL <https://www.mdpi.com/2073-4433/11/11/1157>.

Chuyao Luo, Xutao Li, and Yunming Ye. Pfst-lstm: A spatiotemporal lstm model with pseudoflow prediction for precipitation nowcasting. *IEEE Journal of Selected Topics in Applied Earth Observations and Remote Sensing*, 14: 843–857, 2021. doi:10.1109/JSTARS.2020.3040648.

Muhammad Salman Pathan, Mayank Jain, Yee Hui Lee, Tarek Al Skaif, and Soumyabrata Dev. Efficient forecasting of precipitation using lstm. In *2021 Photonics & Electromagnetics Research Symposium (PIERS)*, pages 2312–2316, 2021. doi:10.1109/PIERS53385.2021.9694772.

Carlos Javier Gamboa-Villafruela, José Carlos Fernández-Alvarez, Maykel Márquez-Mijares, Albenis Pérez-Alarcón, and Alfo José Batista-Leyva. Convolutional lstm architecture for precipitation nowcasting using satellite data. *Environmental Sciences Proceedings*, 8(1), 2021. ISSN 2673-4931. doi:10.3390/ecas2021-10340. URL <https://www.mdpi.com/2673-4931/8/1/33>.

Zi-yi Shen and Wen-chao Ban. Machine learning model combined with ceemdan algorithm for monthly precipitation prediction. *Earth Science Informatics*, 16(2):1821–1833, 06 2023. ISSN 1865-0481. doi:10.1007/s12145-023-01011-w.

Xianghua Wu, Jieqin Zhou, Huaying Yu, Duanyang Liu, Kang Xie, Yiqi Chen, Jingbiao Hu, Haiyan Sun, and Fengjuan Xing. The development of a hybrid wavelet-arima-lstm model for precipitation amounts and drought analysis. *Atmosphere*, 12(1), 2021. ISSN 2073-4433. doi:10.3390/atmos12010074. URL <https://www.mdpi.com/2073-4433/12/1/74>.

Xianqi Zhang, Xilong Wu, Shaoyu He, and Dong Zhao. Precipitation forecast based on ceemd-lstm coupled model. *Water Supply*, 21(8):4641–4657, 07 2021a. ISSN 1606-9749. doi:10.2166/ws.2021.237. URL <https://doi.org/10.2166/ws.2021.237>.

Jie Zhou, Ganqu Cui, Shengding Hu, Zhengyan Zhang, Cheng Yang, Zhiyuan Liu, Lifeng Wang, Changcheng Li, and Maosong Sun. Graph neural networks: A review of methods and applications. *AI Open*, 1:57–81, 2020. ISSN 2666-6510. doi:<https://doi.org/10.1016/j.aiopen.2021.01.001>. URL <https://www.sciencedirect.com/science/article/pii/S2666651021000012>.

Yutong Chen, Ya Wang, Gang Huang, and Qun Tian. Coupling physical factors for precipitation forecast in china with graph neural network. *Geophysical Research Letters*, 51(2):e2023GL106676, 2024. doi:<https://doi.org/10.1029/2023GL106676>. URL <https://agupubs.onlinelibrary.wiley.com/doi/abs/10.1029/2023GL106676>. e2023GL106676 2023GL106676.

Xuan Peng, Qian Li, and Jinrui Jing. Cngat: A graph neural network model for radar quantitative precipitation estimation. *IEEE Transactions on Geoscience and Remote Sensing*, 60:1–14, 2022b. doi:10.1109/TGRS.2021.3120218.

Xiaoni Sun, Yong Zhang, Xinglin Piao, Jiayi Wu, Guodong Jing, and Baocai Yin. Pn-hggn: Precipitation nowcasting network via hypergraph neural networks. *IEEE Transactions on Geoscience and Remote Sensing*, 62:1–12, 2024. doi:10.1109/TGRS.2024.3407157.

Xuan Peng, Qian Li, Lei Chen, Xiangyu Ning, Hai Chu, and Jinqing Liu. A structured graph neural network for improving the numerical weather prediction of rainfall. *Journal of Geophysical Research: Atmospheres*, 128(22):e2023JD039011, 2023. doi:<https://doi.org/10.1029/2023JD039011>. URL <https://agupubs.onlinelibrary.wiley.com/doi/abs/10.1029/2023JD039011>. e2023JD039011 2023JD039011.

Umair Yousaf, Alessio De Rango, Luca Furnari, Donato D'Ambrosio, Alfonso Senatore, and Giuseppe Mendicino. A structured graph neural network for improving the numerical weather prediction of rainfall. *Soft Computing*, 29:4481–4494, 2025.

Minh Khiem Pham, Phi Le Nguyen, Viet Hung Vu, Thao Nguyen Truong, Hoa Vo-Van, and Thanh Ngo-Duc. A data-driven approach for high accurate spatiotemporal precipitation estimation. *Neural Computing and Applications*, 36:6099–6118, 2024.

Remi Lam, Alvaro Sanchez-Gonzalez, Matthew Willson, Peter Wirnsberger, Meire Fortunato, Ferran Alet, Suman Ravuri, Timo Ewalds, Zach Eaton-Rosen, Weihua Hu, Alexander Merose, Stephan Hoyer, George Holland, Oriol Vinyals, Jacklynn Stott, Alexander Pritzel, Shakir Mohamed, and Peter Battaglia. Learning skillful medium-range global weather forecasting. *Science*, 382(6677):1416–1421, 2023. doi:10.1126/science.adi2336.

Zihuang Yan, Xianghui Lu, Lifeng Wu, Fa Liu, Rangjian Qiu, Yaokui Cui, and Xin Ma. Evaluation of precipitation forecasting base on graphcast over mainland china. *Scientific Reports*, 15:14771, 2025. doi:10.1038/s41598-025-98944-7.

Ian J. Goodfellow, Jean Pouget-Abadie, Mehdi Mirza, Bing Xu, David Warde-Farley, Sherjil Ozair, Aaron Courville, and Yoshua Bengio. Generative adversarial nets. In *Proceedings of the 28th International Conference on Neural Information Processing Systems - Volume 2*, NIPS'14, page 2672–2680, Cambridge, MA, USA, 2014. MIT Press.

Shivani Pachika, A. Brahmananda Reddy, Bhavishya Pachika, and Akhil Karnam. Generative adversarial networks: Overview. In B. Rama Devi, Kishore Kumar, M. Raju, K. Srujan Raju, and Mathini Sellathurai, editors, *Proceedings of Fifth International Conference on Computer and Communication Technologies*, pages 319–328, Singapore, 2024. Springer Nature Singapore. ISBN 978-981-99-9704-6.

Negin Hayatbini, Bailey Kong, Kuo-lin Hsu, Phu Nguyen, Soroosh Sorooshian, Graeme Stephens, Charless Fowlkes, Ramakrishna Nemani, and Sangram Ganguly. Conditional generative adversarial networks (cgans) for near real-time precipitation estimation from multispectral goes-16 satellite imageries—persiann-cgan. *Remote Sensing*, 11(19), 2019. ISSN 2072-4292. doi:10.3390/rs11192193. URL <https://www.mdpi.com/2072-4292/11/19/2193>.

Cunguang Wang, Guoqiang Tang, and Pierre Gentine. Precipgan: Merging microwave and infrared data for satellite precipitation estimation using generative adversarial network. *Geophysical Research Letters*, 48(5):e2020GL092032, 2021b. doi:<https://doi.org/10.1029/2020GL092032>. URL <https://agupubs.onlinelibrary.wiley.com/doi/abs/10.1029/2020GL092032> e2020GL092032 2020GL092032.

Liuja Xu, Dan Niu, Tianbao Zhang, Pengju Chen, Xunlai Chen, and Yinghao Li. Two-stage ua-gan for precipitation nowcasting. *Remote Sensing*, 14(23), 2022. ISSN 2072-4292. doi:10.3390/rs14235948. URL <https://www.mdpi.com/2072-4292/14/23/5948>.

Ashish Vaswani, Noam Shazeer, Niki Parmar, Jakob Uszkoreit, Llion Jones, Aidan N. Gomez, Łukasz Kaiser, and Illia Polosukhin. Attention is all you need. In *Proceedings of the 31st International Conference on Neural Information Processing Systems*, NIPS'17, page 6000–6010, Red Hook, NY, USA, 2017. Curran Associates Inc. ISBN 9781510860964.

Abdulaziz Amer Aleissaee, Amandeep Kumar, Rao Muhammad Anwer, Salman Khan, Hisham Cholakkal, Gui-Song Xia, and Fahad Shahbaz Khan. Transformers in remote sensing: A survey. *Remote Sensing*, 15(7), 2023. ISSN 2072-4292. doi:10.3390/rs15071860. URL <https://www.mdpi.com/2072-4292/15/7/1860>.

Alabi Bojesomo, Hasan Al-Marzouqi, and Panos Liatsis. Spatiotemporal vision transformer for short time weather forecasting. In *2021 IEEE International Conference on Big Data (Big Data)*, pages 5741–5746, 2021. doi:10.1109/BigData52589.2021.9671442.

Zhihan Gao, Xingjian Shi, Hao Wang, Yi Zhu, Yuyang Wang, Mu Li, and Dit-Yan Yeung. Earthformer: exploring space-time transformers for earth system forecasting. In *Proceedings of the 36th International Conference on Neural Information Processing Systems*, NIPS '22, Red Hook, NY, USA, 2022a. Curran Associates Inc. ISBN 9781713871088.

Qizhao Jin, Xinbang Zhang, Xinyu Xiao, Ying Wang, Shiming Xiang, and Chunhong Pan. Preformer: Simple and efficient design for precipitation nowcasting with transformers. *IEEE Geoscience and Remote Sensing Letters*, 21: 1–5, 2024. doi:10.1109/LGRS.2023.3325628.

Zhuang Li, Zhenyu Lu, Yizhe Li, and Xuan Liu. Swinnowcast: A swin transformer-based model for radar-based precipitation nowcasting. *Remote Sensing*, 17(9), 2025a. ISSN 2072-4292. doi:10.3390/rs17091550. URL <https://www.mdpi.com/2072-4292/17/9/1550>.

Tian-Bao Li, Yu-Ting Su, Dan Song, Wen-Hui Li, Zhi-Qiang Wei, and An-An Liu. Multi-scale spatial-temporal transformer for meteorological variable forecasting. *IEEE Transactions on Circuits and Systems for Video Technology*, 35(3):2474–2486, 2025b. doi:10.1109/TCST.2024.3487965.

Dawei Li, Kefeng Deng, Di Zhang, Yudi Liu, Hongze Leng, Fukang Yin, Kaijun Ren, and Junqiang Song. Lpt-qpn: A lightweight physics-informed transformer for quantitative precipitation nowcasting. *IEEE Transactions on Geoscience and Remote Sensing*, 61:1–19, 2023a. doi:10.1109/TGRS.2023.3328945.

Md. Jalil Piran, Xiaoding Wang, Ho Jun Kim, and Hyun Han Kwon. Precipitation nowcasting using transformer-based generative models and transfer learning for improved disaster preparedness. *International Journal of Applied Earth Observation and Geoinformation*, 132:103962, 2024. ISSN 1569-8432. doi:<https://doi.org/10.1016/j.jag.2024.103962>. URL <https://www.sciencedirect.com/science/article/pii/S1569843224003169>.

Zewei Zhao, Xichao Dong, Yupei Wang, and Cheng Hu. Advancing realistic precipitation nowcasting with a spatiotemporal transformer-based denoising diffusion model. *IEEE Transactions on Geoscience and Remote Sensing*, 62:1–15, 2024a. doi:10.1109/TGRS.2024.3355755.

ChaoRong Li, XuDong Ling, YiLan Xue, Wenjie Luo, LiHong Zhu, FengQing Qin, Yaodong Zhou, and Yuanyuan Huang. Precipitation nowcasting using diffusion transformer with causal attention. *IEEE Transactions on Geoscience and Remote Sensing*, 62:1–16, 2024a. doi:10.1109/TGRS.2024.3510693.

Hao Cao, Yirui Wu, Yansong Bao, Xi Feng, Shaohua Wan, and Cheng Qian. Utrans-net: A model for short-term precipitation prediction. *Artificial Intelligence and Applications*, 1(2):90–97, Sep. 2022. doi:10.47852/bonviewAIA2202337.

Zewei Zhao, Xichao Dong, Yupei Wang, Jianping Wang, Yubao Chen, and Cheng Hu. Mdtnet: Multiscale deformable transformer network with fourier space losses toward fine-scale spatiotemporal precipitation nowcasting. *IEEE Transactions on Geoscience and Remote Sensing*, 62:1–17, 2024b. doi:10.1109/TGRS.2024.3414934.

Xichao Dong, Zewei Zhao, Yupei Wang, Jianping Wang, and Cheng Hu. Motion-guided global-local aggregation transformer network for precipitation nowcasting. *IEEE Transactions on Geoscience and Remote Sensing*, 60:1–16, 2022. doi:10.1109/TGRS.2022.3217639.

Wenhui Li, Ying Zhou, Yue Li, Dan Song, Zhiqiang Wei, and An-An Liu. Hierarchical transformer with lightweight attention for radar-based precipitation nowcasting. *IEEE Geoscience and Remote Sensing Letters*, 21:1–5, 2024b. doi:10.1109/LGRS.2024.3359229.

Luwen Xu, Jiwei Qin, Dezhi Sun, Yuanyuan Liao, and Jiong Zheng. Pfformer: A time-series forecasting model for short-term precipitation forecasting. *IEEE Access*, 12:130948–130961, 2024. doi:10.1109/ACCESS.2024.3458055.

Lei She, Chenghong Zhang, Xin Man, and Jie Shao. Llmdiff: Diffusion model using frozen llm transformers for precipitation nowcasting. *Sensors*, 24(18), 2024. ISSN 1424-8220. doi:10.3390/s24186049. URL <https://www.mdpi.com/1424-8220/24/18/6049>.

Haoran Bi, Maksym Kyryliuk, Zhiyi Wang, Cristian Meo, Yanbo Wang, Ruben Imhoff, Remko Uijlenhoet, and Justin Dauwels. Nowcasting of extreme precipitation using deep generative models. In *ICASSP 2023 - 2023 IEEE International Conference on Acoustics, Speech and Signal Processing (ICASSP)*, pages 1–5, 2023b. doi:10.1109/ICASSP49357.2023.10094988.

Hongyuan Liu, Qinli Yang, Zhaoyu Liu, Junming Shao, and Guoqing Wang. An attention-mechanism-based deep fusion model for improving quantitative precipitation estimation in a sparsely-gauged basin. *Journal of Hydrology*, 628:130568, 2024. ISSN 0022-1694. doi:<https://doi.org/10.1016/j.jhydrol.2023.130568>. URL <https://www.sciencedirect.com/science/article/pii/S002216942301510X>.

Taisong Xiong, Jianxing He, Hao Wang, Xiaowen Tang, Zhao Shi, and Qiangyu Zeng. Contextual sa-attention convolutional lstm for precipitation nowcasting: A spatiotemporal sequence forecasting view. *IEEE Journal of Selected Topics in Applied Earth Observations and Remote Sensing*, 14:12479–12491, 2021. doi:10.1109/JSTARS.2021.3128522.

Lizhi Tao, Xinguang He, Jiajia Li, and Dong Yang. A multiscale long short-term memory model with attention mechanism for improving monthly precipitation prediction. *Journal of Hydrology*, 602:126815, 2021. ISSN 0022-1694. doi:<https://doi.org/10.1016/j.jhydrol.2021.126815>. URL <https://www.sciencedirect.com/science/article/pii/S0022169421008659>.

Isa Ebtehaj and Hossein Bonakdari. Cnn vs. lstm: A comparative study of hourly precipitation intensity prediction as a key factor in flood forecasting frameworks. *Atmosphere*, 15(9), 2024. ISSN 2073-4433. doi:10.3390/atmos15091082. URL <https://www.mdpi.com/2073-4433/15/9/1082>.

Cong Bai, Feng Sun, Jinglin Zhang, Yi Song, and Shengyong Chen. Rainformer: Features extraction balanced network for radar-based precipitation nowcasting. *IEEE Geoscience and Remote Sensing Letters*, 19:1–5, 2022. doi:10.1109/LGRS.2022.3162882.

S. Pulkkinen, D. Nerini, A. A. Pérez Hortal, C. Velasco-Forero, A. Seed, U. Germann, and L. Foresti. Pysteps: an open-source python library for probabilistic precipitation nowcasting (v1.0). *Geoscientific Model Development*, 12(10):4185–4219, 2019. doi:10.5194/gmd-12-4185-2019. URL <https://gmd.copernicus.org/articles/12/4185/2019/>.

Anirudhan Badrinath, Luca Delle Monache, Negin Hayatbini, Will Chapman, Forest Cannon, and Marty Ralph. Improving precipitation forecasts with convolutional neural networks. *Weather and Forecasting*, 38(2):291–306, 2023. doi:10.1175/WAF-D-22-0002.1. URL <https://journals.ametsoc.org/view/journals/wefo/38/2/WAF-D-22-0002.1.xml>.

Taereem Kim, Tiantian Yang, Lujun Zhang, and Yang Hong. Near real-time hurricane rainfall forecasting using convolutional neural network models with integrated multi-satellite retrievals for gpm (imerg) product. *Atmospheric Research*, 270:106037, 2022. ISSN 0169-8095. doi:<https://doi.org/10.1016/j.atmosres.2022.106037>. URL <https://www.sciencedirect.com/science/article/pii/S0169809522000230>.

Qin Jiang, Francesco Cioffi, Weiyue Li, Jinkai Tan, Xiaoduo Pan, and Xin Li. Hybrid multilayer perceptron and convolutional neural network model to predict extreme regional precipitation dominated by the large-scale atmospheric circulation. *Atmospheric Research*, 304:107362, 2024. ISSN 0169-8095. doi:<https://doi.org/10.1016/j.atmosres.2024.107362>. URL <https://www.sciencedirect.com/science/article/pii/S0169809524001443>.

Weide Li, Xi Gao, Zihan Hao, and Rong Sun. Using deep learning for precipitation forecasting based on spatio-temporal information: a case study. *Climate Dynamics*, 58:443–457, 2022b. ISSN 1432-0894. doi:10.1007/s00382-021-05916-4.

Longfei Guo, Yunwei Pu, and Wenxiang Zhao. Cnn-bilstm daily precipitation prediction based on attention mechanism. *Atmosphere*, 16(3), 2025. ISSN 2073-4433. doi:10.3390/atmos16030333. URL <https://www.mdpi.com/2073-4433/16/3/333>.

Weixin Jin, Yong Luo, Tongwen Wu, Xiaomeng Huang, Wei Xue, and Chaoqing Yu. Deep learning for seasonal precipitation prediction over china. *Journal of Meteorological Research*, 36:271–281, 2022. ISSN 2198-0934. doi:10.1007/s13351-022-1174-7.

Yanbo Gao, Jiping Guan, Fuhan Zhang, Xiaodong Wang, and Zhiyong Long. Attention-unet-based near-real-time precipitation estimation from fengyun-4a satellite imageries. *Remote Sensing*, 14(12), 2022b. ISSN 2072-4292. doi:10.3390/rs14122925. URL <https://www.mdpi.com/2072-4292/14/12/2925>.

Andrew Paul Barnes, Nick McCullen, and Thomas Rodding Kjeldsen. Forecasting seasonal to sub-seasonal rainfall in great britain using convolutional-neural networks. *Theoretical and Applied Climatology*, 151:421–432, 2023. ISSN 1434-4483. doi:10.1007/s00704-022-04242-x.

Jenna Ritvanen, Bent Harnist, Miguel Aldana, Terhi Mäkinen, and Seppo Pulkkinen. Advection-free convolutional neural network for convective rainfall nowcasting. *IEEE Journal of Selected Topics in Applied Earth Observations and Remote Sensing*, 16:1654–1667, 2023. doi:10.1109/JSTARS.2023.3238016.

Lu Yi, Zhangyang Gao, Zhehui Shen, Haitao Lin, Zicheng Liu, Siqi Ma, Cunguang Wang, Stan Z. Li, and Ling Li. Precipitation estimation based on infrared data with a spherical convolutional neural network. *Journal of Hydrometeorology*, 24(4):743–760, 2023. doi:10.1175/JHM-D-22-0081.1. URL <https://journals.ametsoc.org/view/journals/hydr/24/4/JHM-D-22-0081.1.xml>.

Tianyi Nan, Jie Chen, Zhiwei Ding, Wei Li, and Hua Chen. Deep learning-based multi-source precipitation merging for the tibetan plateau. *Science China Earth Sciences*, 66:852–870, 2023. ISSN 1869-1897. doi:10.1007/s11430-022-1050-2.

Jongyun Byun, Changhyun Jun, Jinwon Kim, Jaehoon Cha, and Roya Narimani. Deep learning-based rainfall prediction using cloud image analysis. *IEEE Transactions on Geoscience and Remote Sensing*, 61:1–11, 2023. doi:10.1109/TGRS.2023.3263872.

Duong Thuy Bui, Truong Xuan Ngo, Thanh Thi Nhat Nguyen, Anh Duc Hoang Gia, Bui Thi Khanh Hoa, Hoang Anh Nguyen-Thi, Tan Van Phan, Federico Porcu, and An Hung Nguyen. Near-real-time integration of multisource precipitation products using a multiscale convolutional neural network. *Journal of Hydrometeorology*, 26(7):1017–1035, 2025. doi:10.1175/JHM-D-24-0120.1. URL <https://journals.ametsoc.org/view/journals/hydr/26/7/JHM-D-24-0120.1.xml>.

Chen Zhang, Zachary P. Brodeur, Scott Steinschneider, and Jonathan D. Herman. Leveraging spatial patterns in precipitation forecasts using deep learning to support regional water management. *Water Resources Research*, 58(9):e2021WR031910, 2022. doi:<https://doi.org/10.1029/2021WR031910>. URL <https://agupubs.onlinelibrary.wiley.com/doi/10.1029/2021WR031910> e2021WR031910 2021WR031910.

He Fu, Jianing Guo, Chenguang Deng, Heng Liu, Jie Wu, Zhenguo Shi, Cailing Wang, and Xiaoning Xie. Deep-learning-based downscaling of precipitation in the middle reaches of the yellow river using residual-based cnns. *Quarterly Journal of the Royal Meteorological Society*, 150(763):3290–3304, 2024. doi:<https://doi.org/10.1002/qj.4759>. URL <https://rmets.onlinelibrary.wiley.com/doi/10.1002/qj.4759>.

Zhifeng Ma, Hao Zhang, and Jie Liu. Preciplstm: A meteorological spatiotemporal lstm for precipitation nowcasting. *IEEE Transactions on Geoscience and Remote Sensing*, 60:1–8, 2022. doi:10.1109/TGRS.2022.3198222.

Shaojie You, Xiaodan Zhang, Hongyu Wang, Chen Quan, Tong Zhao, Chang Liu, Wei Huo, Qiyuan Zhang, and Naihao Hu. A multisource precipitation data fusion model for qinghai province based on 3d cnn and bidirectional convlstm. *Journal of Hydrometeorology*, 26(3):327–343, 2025. doi:10.1175/JHM-D-24-0053.1. URL <https://journals.ametsoc.org/view/journals/hydr/26/3/JHM-D-24-0053.1.xml>.

Xinyun Jiang. A combined monthly precipitation prediction method based on ceemd and improved lstm. *PLOS ONE*, 18(7):1–18, 07 2023. doi:10.1371/journal.pone.0288211. URL <https://doi.org/10.1371/journal.pone.0288211>.

Xuefei Cui, Zhaocai Wang, and Renlin Pei. A vmd-msma-lstm-arima model for precipitation prediction. *Hydrological Sciences Journal*, 68(6):810–839, 2023. doi:10.1080/02626667.2023.2190896.

Shaolei Guo, Shifeng Sun, Xianqi Zhang, Haiyang Chen, and Haiyang Li. Monthly precipitation prediction based on the emd–vmd–lstm coupled model. *Water Supply*, 23(11):4742–4758, 10 2023. ISSN 1606-9749. doi:10.2166/ws.2023.275. URL <https://doi.org/10.2166/ws.2023.275>.

Suting Chen, Xin Xu, Yanyan Zhang, Dongwei Shao, Song Zhang, and Mingjian Zeng. Two-stream convolutional lstm for precipitation nowcasting. *Neural Computing and Applications*, 34:13281–13290, 2022. ISSN 1433-3058. doi:10.1007/s00521-021-06877-9.

Fuzeng Wang, Yaxi Cao, Qiusong Wang, Tong Zhang, and Debin Su. Estimating precipitation using lstm-based raindrop spectrum in guizhou. *Atmosphere*, 14(6), 2023. ISSN 2073-4433. doi:10.3390/atmos14061031. URL <https://www.mdpi.com/2073-4433/14/6/1031>.

Xuying Yang, Feng Zhang, Peng Sun, Xiaofan Li, Zhenhong Du, and Renyi Liu. A spatio-temporal graph-guided convolutional lstm for tropical cyclones precipitation nowcasting. *Applied Soft Computing*, 124:109003, 2022. ISSN 1568-4946. doi:<https://doi.org/10.1016/j.asoc.2022.109003>. URL <https://www.sciencedirect.com/science/article/pii/S1568494622003258>.

Jiwei Zhao, Guangzheng Nie, and Yihao Wen. Monthly precipitation prediction in luoyang city based on eemd-lstm-arima model. *Water Science and Technology*, 87(1):318–335, 12 2022. ISSN 0273-1223. doi:10.2166/wst.2022.425. URL <https://doi.org/10.2166/wst.2022.425>.

Chuyao Luo, Xutao Li, Yunming Ye, Shanshan Feng, and Michael K. Ng. Experimental study on generative adversarial network for precipitation nowcasting. *IEEE Transactions on Geoscience and Remote Sensing*, 60:1–20, 2022a. doi:10.1109/TGRS.2022.3177625.

Jingnan Wang, Xiaodong Wang, Jiping Guan, Lifeng Zhang, Fuhan Zhang, and Tao Chang. Stpf-net: Short-term precipitation forecast based on a recurrent neural network. *Remote Sensing*, 16(1), 2024. ISSN 2072-4292. doi:10.3390/rs16010052. URL <https://www.mdpi.com/2072-4292/16/1/52>.

Chuyao Luo, Xinyue Zhao, Yuxi Sun, Xutao Li, and Yunming Ye. Predrann: The spatiotemporal attention convolution recurrent neural network for precipitation nowcasting. *Knowledge-Based Systems*, 239:107900, 2022b. ISSN 0950-7051. doi:<https://doi.org/10.1016/j.knosys.2021.107900>. URL <https://www.sciencedirect.com/science/article/pii/S0950705121010601>.

Qian Liu, Yongxiang Xiao, Yaocheng Gui, Guilan Dai, Haoran Li, Xu Zhou, Aiai Ren, Guoqiang Zhou, and Jun Shen. Mmf-rnn: A multimodal fusion model for precipitation nowcasting using radar and ground station data. *IEEE Transactions on Geoscience and Remote Sensing*, 63:1–16, 2025. doi:10.1109/TGRS.2025.3528423.

Nan Yang, Chong Wang, and Xiaofeng Li. Evaluation of precipitation forecasting methods and an advanced lightweight model. *Environmental Research Letters*, 19(9), 2024. doi:10.1088/1748-9326/ad661f.

Wenyan Li, Haonan Chen, and Lei Han. Polarimetric radar quantitative precipitation estimation using deep convolutional neural networks. *IEEE Transactions on Geoscience and Remote Sensing*, 61:1–11, 2023b. doi:10.1109/TGRS.2023.3280799.

Xianqi Zhang, Yang Yang, Jiawen Liu, Yuehan Zhang, and Yupeng Zheng. A cnn-bilstm monthly rainfall prediction model based on scssa optimization. *Journal of Water and Climate Change*, 15(9):4862–4876, 09 2024. ISSN 2040-2244. doi:10.2166/wcc.2024.389. URL <https://doi.org/10.2166/wcc.2024.389>.

Yuhang Zhang, Aizhong Ye, Phu Nguyen, Bita Analui, Soroosh Sorooshian, and Kuolin Hsu. New insights into error decomposition for precipitation products. *Geophysical Research Letters*, 48(17):e2021GL094092, 2021b. doi:<https://doi.org/10.1029/2021GL094092>. URL <https://agupubs.onlinelibrary.wiley.com/doi/abs/10.1029/2021GL094092>. e2021GL094092 2021GL094092.